

Adaptive Control and Reconfiguration of Mobile Wireless Sensor Networks for Dynamic Multi-Target Tracking

Xi Zhang, *Senior Member, IEEE*

Abstract—We propose the adaptive control and reconfiguration schemes for mobile wireless sensor networks (MWSN) to achieve timely and accurate mobile multi-target tracking (MMTT) with cost-effective energy consumption. In particular, our proposed schemes can detect the mobile multi-targets' random appearance and disappearance in the clutter environments with high accuracy and low energy cost. We develop the optimal mutual-information based techniques to adaptively control the reconfiguration of the proposed MWSN by designing the Distributed/Decentralized Probability Hypothesis Density (DPHD) filtering algorithms. By dynamically adjusting the sensors' states, including their positions and activations, our schemes can efficiently improve the observabilities of the tracked multi-targets. We further analyze the asymptotic performance of our proposed schemes by deriving the upper-bounds of the detection-error probabilities. Also presented are the performance analyses which validate and evaluate our proposed adaptive control and reconfiguration schemes for MWSN in terms of the multi-target states estimation accuracy, the energy-consumption efficiency, and the robustness to the interference/noise.

Index Terms—Distributed/Decentralized Probability Hypothesis Density (DPHD) Filter, dynamic mobile multi-target tracking, mobile wireless sensor networks (MWSN), mutual information-theory based control.

I. INTRODUCTION

IN the clutter environments, Mobile Multiple Targets Tracking (MMTT) is a promising technique to accurately estimate the number of mobile targets, which is typically time-varying, and their dynamic activities [1], [2]. Consequently, MMTT has received more and more research attention. Recently, Wireless Sensor Networks (WSN) have proven to be the effective approach in solving the MMTT problem [3], [4]. On the one hand, abundant information can be conveniently obtained through a large number of sensor nodes supporting wireless transmissions. On the other hand, the independent locations of distributed sensor nodes significantly enlarge the coverage areas for MMTT. However, how to efficiently use WSN to implement MMTT still faces many challenges. First, achieving accurate estimation for MMTT in WSN usually

requires highly-effective collaboration among sensor nodes. Second, since the sensors use battery power supplies, the collaboration and transmission schemes of the WSN for MMTT need to be energy efficient. Third, for the WSN with mobile sensor nodes, the sensor-node reconfiguration needs to be dynamically performed through the distributed control algorithms, such that MMTT can adapt to the diverse activities of the mobile targets.

There have been various schemes proposed for MMTT in WSN. Finite set statistics (FISST) introduced in [5] provides an efficient framework for MMTT by using the Random Finite Set (RFS) theory. Based on FISST, Probability Hypothesis Density (PHD) filter recursively updates the first-order moment (also called the intensity function) associated with the multi-target posterior at each time step [6]. For tracking the time-varying number of targets, the PHD filter's computational complexity is much less than the conventional joint probabilistic data association filter. The Gaussian-mix PHD filter and particle PHD filter are the two main types of PHD filters [7], [8]. The particle PHD filter uses the highly nonlinear measurement models and thus is more efficient in solving the MMTT problem as compared with the Gaussian-mix PHD filter. To enhance the efficiency of the particle PHD filter, several variants of the particle PHD filter have been developed, such as the auxiliary particle PHD filter and Rao-blackwellised particle PHD filter [9], [10]. However, the above works mainly focus on improving the multi-target state estimation accuracy obtained by the individual sensors. However, and they did not consider the collaboration strategy among the sensors.

To track the multiple targets with high accuracy, the control system needs to have the abilities of determining the sensor nodes' activations and collaborations. Various sensor-collaboration controlling schemes for the target-tracking problem have been developed in [11]–[14]. In [11], the authors derived an entropy-based information utility function for the sensor activation problem, and also proposed an efficient numerical solution for the centralized data fusion. The research in [12] develops an information-driven controlling scheme for the parallel-structured WSN by using the particle filtering algorithm. However, these works concentrate only on the single target tracking problem, which cannot be directly applied to the MMTT problem.

The authors in [13] developed a dynamic sensor self-organization scheme for the MMTT problem. This sensor-controlling scheme groups the sensor nodes into non-overlapping clusters which track the targets independently. This scheme is effective when the mobile targets are far from each other. But, it cannot effectively distinguish the individual targets when they

Manuscript received April 17, 2011; revised May 01, 2011; accepted July 25, 2011. Date of publication August 08, 2011; date of current version October 05, 2011. This work was supported in part by the National Science Foundation CAREER Award under Grant ECS-0348694. Recommended by Associate Editor J. Chen.

The author is with the Networking and Information Systems Laboratory, Department of Electrical and Computer Engineering, Texas A&M University, College Station, TX 77843 USA (e-mail: xizhang@ece.tamu.edu).

Digital Object Identifier 10.1109/TAC.2011.2163862

are close to each other. Our previous work in [14] developed a hierarchical wireless sensor network and the corresponding sensor-collaboration schemes, which can obtain the high multi-target states estimation accuracy in both of the above two cases. While the above schemes can achieve effective control and accurate estimation for the MMTT problem, they do not take the energy-consumption issue into account. As a consequence, the lifetime of WSN may be severely shortened, significantly degrading the performances of MMTT.

To overcome the aforementioned problems, we develop the efficient distributed Mobile Wireless Sensor Networks (MWSN)-based control system using our proposed Distributed/Decentralized Probability Hypothesis Density (DPHD) filtering algorithm, which detect the random appearance and disappearance of the mobile multi-targets with high estimation accuracy and low energy consumption. In particular, we focus on a two-tier hierarchical MWSN consisting of the mobile sensor nodes acting as the Cluster Heads (CH) and the static sensor nodes acting as the cluster members. In our proposed sensor-control system, we develop the optimal mutual information utility based techniques to adaptively control the locations of the CHs, the activations of the CHs and the cluster members, and their collaboration schemes. At each time step, all the available CHs locally determine their candidate locations by jointly minimizing the side-effect impacts of the movements and maximizing the predicted information gain on the multi-target states. After moving to the new location, each CH activates the static sensor nodes located within its communication range by minimizing the predicted energy consumption for future target-tracking while ensuring the predicted multi-target states estimation accuracy is above some pre-defined threshold. The active sensor nodes act as the new cluster members, which detect the tracked targets and send their local measurements to their CHs. The CHs quantize and encode the raw data locally by using the Huffman tree [16], filter the information considered as the false alarms, and send the remains to the global Fusion Center (FC), which reconstructs the detection information and makes a final estimation of the multi-target states.

The rest of this paper is organized as follows. Section II describes our MWSN-based control system models. Section III proposes the Distributed/Decentralized Probability Hypothesis Density (DPHD) filtering algorithm. Section IV derives the optimal Cluster Head (CH)-movement controlling scheme. Section V develops our cluster-member activation scheme. Section VI analyzes the asymptotic performance of our proposed MWSN-based control system. Section VII validates and evaluates our proposed MWSN-based control system and our proposed DPHD filtering algorithm in terms of the multi-target states estimation accuracy and the total energy consumption through extensive simulations. The paper concludes with Section VIII.

II. SYSTEM MODELS

To track the multiple mobile targets accurately with low energy consumption and communication load, we consider a *two-tier hierarchical* MWSN, which consists of N_c mobile sensor nodes acting as the Cluster Heads (CHs) and N_s static sensor

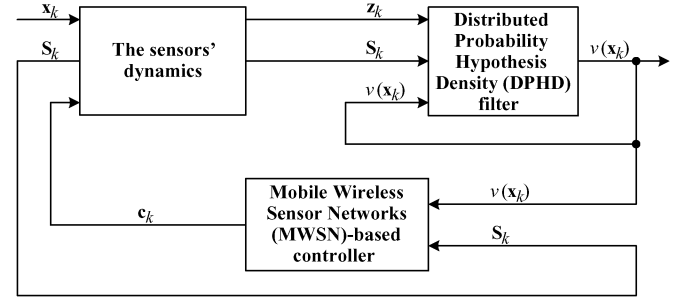


Fig. 1. Architecture of our proposed adaptive control and reconfiguration scheme for MWSN.

nodes acting as the cluster members under a mobile Cluster Head (CH). The MWSN is responsible for tracking the number and the trajectories of the multiple mobile targets. In particular, the cluster members measure the states of the mobile targets, and forward the obtained information to their CHs. The CHs fuse and quantize the collected information from the cluster members, which will then be transmitted to the global fusion center for the final estimation of the mobile targets' states. As shown in Fig. 1, our proposed MWSN-based MMTT control-system architecture is composed of the following three main parts: 1) the sensors' dynamics, 2) the DPHD filter, and 3) the MWSN-based controller. We denote the states of all sensors, the states of all mobile targets, and the measurements of all sensors by the Random Finite Sets (RFS) s_k , x_k and z_k , respectively, (RFS and these variables will be elaborated on later), where k is the time step index. Moreover, c_k in Fig. 1 is the control vector generated by the MWSN-based controller. Based on their states s_k , the active sensor nodes detect the multi-target states x_k and obtain the sensing measurements z_k . To estimate the mobile multi-target states by using the sensing measurements, we develop the DPHD filter to obtain the first-order moment of the multi-target states, called the posterior intensity $\nu(x_k)$, and propagate $\nu(x_k)$ to the next time step. The sensors' current states and the posterior intensity of the multi-target states are the inputs of our proposed MWSN-based controller which controls the movement and the activation of the available mobile sensor nodes and the memberships of the static sensor nodes.

The objective of our control system is to minimize the distance between the exact posterior density of the mobile multi-target states and the estimated posterior density of the mobile multi-target states. This can be achieved through maximizing the likelihood of tracking the mobile multi-target states, which in the meantime minimizes the expected number of future observations required to track the mobile multi-target states. Furthermore, the above optimization equivalently minimizes the expected log-likelihood of the posterior density with each set of the mobile multi-target states estimations. Thus, extending the mutual information based techniques for the single-target tracking [12] and applying the notion of the posterior intensity obtained by our DPHD filtering algorithms [14], we can formulate our optimization problem for mobile multi-target tracking as follows:

$$\min_{c_k} \{H(x_k|z_k)\} = \min_{c_k} \{H(x_k) - I(x_k; z_k)\} \quad (1)$$

where

$$\begin{cases} H(\mathbf{x}_k) = - \int_{\mathbf{x}_k \in \mathbf{X}} \nu(\mathbf{x}_k) \log \nu(\mathbf{x}_k) d\mathbf{x}_k, \\ H(\mathbf{x}_k | \mathbf{z}_k) = - \int_{\mathbf{z}_k \in \mathbf{Z}} \int_{\mathbf{x}_k \in \mathbf{X}} \nu(\mathbf{x}_k, \mathbf{z}_k) \log \nu(\mathbf{x}_k | \mathbf{z}_k) d\mathbf{x}_k d\mathbf{z}_k, \\ I(\mathbf{x}_k; \mathbf{z}_k) = \int_{\mathbf{z}_k \in \mathbf{Z}} \int_{\mathbf{x}_k \in \mathbf{X}} \nu(\mathbf{x}_k, \mathbf{z}_k) \log \frac{\nu(\mathbf{x}_k, \mathbf{z}_k)}{\nu(\mathbf{x}_k)\nu(\mathbf{z}_k)} d\mathbf{x}_k d\mathbf{z}_k \end{cases}$$

and \mathbf{c}_k is the output vector of the MWSN-based controller as depicted in Fig. 1. We can further simplify the optimization problem specified in (1) as follows:

$$\max_{\mathbf{c}_k} \{I(\mathbf{x}_k; \mathbf{z}_k)\}. \quad (2)$$

Equation (2) implies that to optimally control and reconfigure the MWSN, we need to compute the output vector of MWSN-based controller \mathbf{c}_k to maximize the mutual information $I(\mathbf{x}_k; \mathbf{z}_k)$. Based on the general optimization problem formulation for mobile multi-target tracking given in (1), we can define the *Mutual Information Utility Function* for the i th mobile sensor in the following.

Definition 1: We define the *Mutual Information Utility Function* for the i th mobile sensor node in the mobile multi-target tracking model give in (1), denoted by $\mathcal{M}^{(i)}(\mathbf{s}_k, \mathbf{c}_k, \nu_k(\mathbf{x}_k))$, as follows:

$$\mathcal{M}^{(i)}(\mathbf{s}_k, \mathbf{c}_k, \nu_k(\mathbf{x}_k)) \triangleq I(\mathbf{x}_k; \mathbf{z}_k^{(i)}). \quad (3)$$

The mutual information between the random variables \mathbf{x}_k and \mathbf{z}_k can be used to evaluate the expected reduction of uncertainty. However, the computational complexity of using a Random Finite Set (RFS) representation to evaluate this quantity increases exponentially with the cardinalities of mobile multi-target states \mathbf{x}_k and measurements of all sensors \mathbf{z}_k . To decrease the computational complexity, we mainly focus on the interactions between the neighboring sensors (pairwise-cooperation) and approximate the mutual information utility function defined in (3) by its (pairwise-node) approximation expression [12]

$$\begin{aligned} \mathcal{M}_p^{(i)}(\mathbf{s}_k, \mathbf{c}_k, \nu(\mathbf{x}_k)) &= \sum_{j=1, j \neq i}^{N_s} \left\{ I(\mathbf{x}_k; \mathbf{z}_k^{(i)}, \mathbf{z}_k^{(j)}) \right\} \\ &\quad - (N_s - 2) \left\{ I(\mathbf{x}_k; \mathbf{z}_k^{(i)}) \right\} \end{aligned} \quad (4)$$

where $N_s \geq 2$; otherwise, we will use (3). To show how $\mathcal{M}_p^{(i)}(\mathbf{s}_k, \mathbf{c}_k, \nu_k(\mathbf{x}_k))$ is close to its exact value of $\mathcal{M}^{(i)}(\mathbf{s}_k, \mathbf{c}_k, \nu_k(\mathbf{x}_k))$, the following (5) and (6) can be shown to be valid to calculate the difference, denoted by $\epsilon_p^{(i)}$, between the exact mutual-information value evaluated at the i th active mobile sensor node by using (3) and the approximation value obtained by using (4):

$$\epsilon_p^{(i)} \triangleq \mathcal{M}^{(i)}(\mathbf{s}_k, \mathbf{c}_k, \nu_k(\mathbf{x}_k)) - \mathcal{M}_p^{(i)}(\mathbf{s}_k, \mathbf{c}_k, \nu_k(\mathbf{x}_k)) \quad (5)$$

$$= \sum_{j=2, j \neq i}^{N_s} I(\mathbf{z}_k^{(j)}; \mathbf{z}_k^{(1)}, \dots, \mathbf{z}_k^{(j-1)} | \mathbf{z}_k^{(i)}) \quad (6)$$

where (5) and (6) can be proved as follows. Without loss of generality, we approximate the mutual information by using the first

(i.e., $i = 1$) mobile sensor node's current detection result. Then, applying mutual information chain rule [16], we can expand the mutual information into the following expressions:

$$\begin{aligned} I(\mathbf{x}_k; \mathbf{z}_k) &= \sum_{j=1}^{N_s} \left\{ I(\mathbf{x}_k; \mathbf{z}_k^{(j)} | \mathbf{z}_k^{(1)}, \mathbf{z}_k^{(2)}, \dots, \mathbf{z}_k^{(j-1)}) \right\} \\ &= I(\mathbf{x}_k; \mathbf{z}_k^{(1)}) \\ &\quad + \sum_{j=2}^{N_s} \left\{ I(\mathbf{x}_k; \mathbf{z}_k^{(1)}, \mathbf{z}_k^{(j)} | \mathbf{z}_k^{(2)}, \dots, \mathbf{z}_k^{(j-1)}) \right. \\ &\quad \left. - I(\mathbf{x}_k; \mathbf{z}_k^{(1)} | \mathbf{z}_k^{(2)}, \dots, \mathbf{z}_k^{(j-1)}) \right\}. \end{aligned} \quad (7)$$

Using the notion of conditional mutual information and its commutative properties [16] for any three random variables \mathcal{X} , \mathcal{Y} , and \mathcal{Z} , we can get the following commutative identities:

$$\begin{cases} I(\mathcal{X}; \mathcal{Y} | \mathcal{Z}) = I(\mathcal{X}; \mathcal{Y}) - I(\mathcal{X}; \mathcal{Z}) + I(\mathcal{X}; \mathcal{Z} | \mathcal{Y}), \\ I(\mathcal{X}; \mathcal{Y} | \mathcal{Z}) = I(\mathcal{X}; \mathcal{Y}) - I(\mathcal{Y}; \mathcal{Z}) + I(\mathcal{Y}; \mathcal{Z} | \mathcal{X}). \end{cases} \quad (8)$$

Applying the identities given by (8), we can rewrite (7) as follows:

$$\begin{aligned} I(\mathbf{x}_k; \mathbf{z}_k) &= \mathcal{M}_p^{(1)}(\mathbf{s}_k, \mathbf{c}_k, \nu(\mathbf{x}_k)) \\ &\quad + \sum_{j=3}^{N_s} \left\{ I(\mathbf{x}_k; \mathbf{z}_k^{(2)}, \dots, \mathbf{z}_k^{(j-1)} | \mathbf{z}_k^{(1)}, \mathbf{z}_k^{(j)}) \right. \\ &\quad \left. - I(\mathbf{x}_k; \mathbf{z}_k^{(2)}, \dots, \mathbf{z}_k^{(j-1)} | \mathbf{z}_k^{(1)}) \right\}. \end{aligned} \quad (9)$$

Given the current mobile multi-target states, the obtained mobile multi-target states detection results are independent. Then, repeatedly using the commutative identities given in (8) again and canceling the terms summing to zero, we can further simplify (9) as follows:

$$\begin{aligned} I(\mathbf{x}_k; \mathbf{z}_k) &= \mathcal{M}_p^{(1)}(\mathbf{s}_k, \mathbf{c}_k, \nu(\mathbf{x}_k)) \\ &\quad + \sum_{j=2}^{N_s} I(\mathbf{z}_k^{(j)}; \mathbf{z}_k^{(1)}, \dots, \mathbf{z}_k^{(j-1)} | \mathbf{z}_k^{(1)}). \end{aligned} \quad (10)$$

Because we consider the MMTT problem in the homogeneous MWSN, we can use the similar approach to obtain

$$I(\mathbf{x}_k; \mathbf{z}_k) = \mathcal{M}_p^{(i)}(\mathbf{s}_k, \mathbf{c}_k, \nu(\mathbf{x}_k)) + \epsilon_p^{(i)} \quad (11)$$

where

$$\epsilon_p^{(i)} = \sum_{j=2, j \neq i}^{N_s} I(\mathbf{z}_k^{(j)}; \mathbf{z}_k^{(1)}, \dots, \mathbf{z}_k^{(j-1)} | \mathbf{z}_k^{(i)}) \quad (12)$$

which completes the proof for (5) and (6).

Therefore, when the active sensor nodes' detection results are not highly correlated, we only need to consider the interactions between the neighboring sensors. Also note that in realistic systems, the detection results of the active sensor nodes typically have low correlations due to the highly spacial-varying wireless fading channels.

In our MWSN-based control system, we define the multi-target states' dynamics model $\mathbf{x}_k^{(i)}$, the sensors' dynamics model

\mathbf{s}_k , and the sensors' measurements model \mathbf{z}_k , respectively, as follows:

$$\begin{cases} \mathbf{x}_k^{(i)} = \begin{bmatrix} 1 & \Delta t & 0 & 0 \\ 0 & 1 & 0 & 0 \\ 0 & 0 & 1 & \Delta t \\ 0 & 0 & 0 & 1 \end{bmatrix} \mathbf{x}_{k-1}^{(i)} + \mathbf{Q}\mathbf{u}_{k-1}, \\ \mathbf{s}_k = f_k(\mathbf{s}_{k-1}, \mathbf{c}_{k-1}), \\ \mathbf{z}_k = h_k(\mathbf{x}_k, \mathbf{s}_k) + \mathbf{v}_k \end{cases} \quad (13)$$

where $\mathbf{x}_k^{(i)} = [x_k^{(i)}, y_k^{(i)}, \dot{x}_k^{(i)}, \dot{y}_k^{(i)}]^T$ with $[x_k^{(i)}, y_k^{(i)}]^T$ denoting the i th target's position at the time step k and $[\dot{x}_k^{(i)}, \dot{y}_k^{(i)}]^T$ being its velocities at time step k , $\mathbf{x}_k = \{\mathbf{x}_k^{(1)}, \mathbf{x}_k^{(2)}, \dots, \mathbf{x}_k^{(n_{x,k})}\}$ denotes the states of all mobile targets, $n_{x,k}$ is the number of the mobile targets, Δt is the sampling period, q is the factor used to control the intensity of the target-state evolution noise, \mathbf{s}_k represents the vector of the active sensors' states, \mathbf{c}_{k-1} denotes the vector of the control inputs at the preceding time step, $f_k(\cdot, \cdot)$ is the dynamic function of the sensors' states, \mathbf{z}_k is the vector of multi-target states measurements, \mathbf{v}_k is the measurement noise vector, $h_k(\cdot, \cdot)$ denotes the measurement function, and

$$\mathbf{Q} = \sqrt{q} \begin{bmatrix} \frac{\Delta t^3}{3} & \frac{\Delta t^2}{2} & 0 & 0 \\ \frac{\Delta t^2}{2} & \Delta t & 0 & 0 \\ 0 & 0 & \frac{\Delta t^3}{3} & \frac{\Delta t^2}{2} \\ 0 & 0 & \frac{\Delta t^2}{2} & \Delta t \end{bmatrix}^{1/2}. \quad (14)$$

To reconfigure the optimal hierarchical Mobile Wireless Sensor Networks (MWSN), we define the control input $\mathbf{c}_{k-1} = [\mathbf{c}_{k-1}^{(1)}, \mathbf{c}_{k-1}^{(2)}, \dots, \mathbf{c}_{k-1}^{(N_s)}]^T$ as a vector with the component $\mathbf{c}_{k-1}^{(i)}$ including the location and the activation status of the i th sensor nodes at time step $(k-1)$, where N_s denotes the total number of the available sensor nodes.

III. DISTRIBUTED PARTICLE HYPOTHESIS DENSITY FILTERING ALGORITHM

A. Random Finite Set Model for Multi-Target Tracking

The MMTT problem can be modeled by (Random Finite Set) RFS framework. Letting χ be the state space of the single target and $n_{x,k}$ be the number of targets at time step k , we can represent the multi-target states at time step k as $\mathbf{x}_k \in F(\chi)$, where $F(\chi)$ denotes the collection of all the finite subsets of χ . For a multi-target states \mathbf{x}_{k-1} at time step $(k-1)$, each component $\mathbf{x}_{k-1}^{(i)}$ either continues to exist at time step k with the probability equal to $p_{S,k}(\mathbf{x}_{k-1}^{(i)})$, or dies with the probability equal to $(1 - p_{S,k}(\mathbf{x}_{k-1}^{(i)}))$. Therefore, given a state \mathbf{x}_k at time step $(k-1)$, we can model its behavior at next time step using the RFS $S_{k|k-1}(\mathbf{x}_k^{(i)})$, which is equal to $\{\mathbf{x}_k^{(i)}\}_{i=1}^{(n_{x,k})}$ when the target survives, and becomes the empty set \emptyset when the target dies. A new target at time step k can appear either by the spontaneous births which can be modeled by Γ_k , or by spawning from $\mathbf{x}_{i,k-1}$ which can be modeled by $B_{k|k-1}(\mathbf{x}_{k-1}^{(i)})$. Given a multi-target

state \mathbf{x}_{k-1} at time step $(k-1)$, we derive the multi-target states \mathbf{x}_k at time step k as follows:

$$\mathbf{x}_k = \left[\bigcup_{\zeta \in \mathbf{x}_{k-1}} S_{k|k-1}(\zeta) \right] \cup \left[\bigcup_{\zeta \in \mathbf{x}_{k-1}} B_{k|k-1}(\zeta) \right] \cup \Gamma_k. \quad (15)$$

Similarly, we denote the measurement-set collected by the j th sensor at time step k as $\mathbf{z}_k^{(j)} \in F(\mathbf{Z}^{(j)})$. A given target state $\mathbf{x}_k^{(i)} \in \mathbf{x}_k$ is either detected with the probability of $p_{D,k}(\mathbf{x}_k^{(i)})$ or missed with the probability of $(1 - p_{D,k}(\mathbf{x}_k^{(i)}))$. Correspondingly, we can model the measurement from the target state $\mathbf{x}_k^{(i)}$ at the j th sensor using the RFS $\Theta_k^{(j)}(\mathbf{x}_k^{(i)})$, which can take on either $\{\mathbf{z}_k^{(j)}\}_{j=1}^{N_s}$ when the target is detected, or the empty set \emptyset otherwise. The j th sensor node can also receive a set of clutter $\mathcal{C}_k^{(j)}$. Thus, given a multi-target states \mathbf{x}_k at time step k , the measurement-set collected by the j th sensor is determined by

$$\mathbf{z}_k^{(j)} = \left[\bigcup_{\mathbf{x} \in \mathbf{x}_k} \Theta_k^{(j)}(\mathbf{x}) \right] \cup \mathcal{C}_k^{(j)}. \quad (16)$$

Letting N_s be the number of the static sensors, we can model the RFS of measurements at time step k as follows:

$$\mathbf{z}_k = \left\{ \mathbf{z}_k^{(1)}, \mathbf{z}_k^{(2)}, \dots, \mathbf{z}_k^{(N_s)} \right\}. \quad (17)$$

B. Probability Hypothesis Density (PHD) Filter

The PHD filter is developed to propagate the posterior intensity, denoted by $\nu(\mathbf{x}_k)$, a first-order statistical moment of the posterior multi-target states, which can be propagated in time via the PHD recursion as follows:

1). The predicting step:

$$\begin{aligned} (\nu_{k|k-1})(\mathbf{x}_k) &= \int p_{S,k}(\zeta) f_{k|k-1}(\mathbf{x}_k|\zeta) d\zeta \\ &+ \int \beta_{k|k-1}(\mathbf{x}_k|\zeta) \nu_{k|k-1}(\zeta) d\zeta + \gamma_k(\mathbf{x}_k) \end{aligned} \quad (18)$$

2). The updating step:

$$\begin{aligned} (\Psi_k \nu_k)(\mathbf{x}_k) &= [1 - p_{D,k}(\mathbf{x}_k)] \nu_k(\mathbf{x}_k) \\ &+ \sum_{\mathbf{z}_k \in \mathbf{Z}_k} \frac{p_{D,k}(\mathbf{x}_k) \eta_k(\mathbf{z}_k|\mathbf{x}_k) \nu_k(\mathbf{x}_k)}{\kappa_k(\mathbf{z}_k) + \int p_{D,k}(\zeta) \eta_k(\mathbf{z}_k|\zeta) \nu_k(\zeta) d\zeta} \end{aligned} \quad (19)$$

where \mathbf{Z}_k is the sensor-measurement space, $f_{k|k-1}(\cdot|\zeta)$ denotes the single target transition PDF, $\gamma_k(\cdot)$ is the intensity of the spontaneous birth RFS, $\beta_{k|k-1}(\cdot|\zeta)$ represents the intensity of the spawning birth RFS, $p_{S,k}(\zeta)$ denotes the probability that a target continues to exist given that its previous state is ζ , Ψ_k is the PHD update operator to generate $\nu_k(\mathbf{x}_k)$, $\eta_k(\cdot|\mathbf{x}_k)$ is the single target measurement likelihood, $p_{D,k}(\mathbf{x}_k)$ denotes the detection probability given a state \mathbf{x}_k , and $\kappa_k(\cdot)$ is the intensity of the clutter RFS. Note that $\kappa_k(\cdot) = \mu_{c,k} p_{c,k}(\cdot)$, where $\mu_{c,k}$ is the average number of clutter points per scan and $p_{c,k}(\cdot)$ is the probability distribution function of each clutter point. The local maxima of the intensity $\nu_k(\mathbf{x}_k)$ are points in χ with the highest local concentration of expected number of elements, and hence can be used to generate estimates for the elements of χ . Thus,

TABLE I
PARTICLE PHD FILTERING ALGORITHM

1. Initialization

◇ Draw L_0 particles from the prior PHD and assign weights:
 $\omega_0^{(i)} = \frac{n_{x,k-1}}{L_0}$, where $n_{x,k-1}$ denotes the prior estimation of target number.

2. At time step $k \geq 1$

◇ According to the proposal densities $q_k(\cdot|\mathbf{x}_{k-1}^{(i)}, \mathbf{z}_k)$ and $p_k(\cdot|\mathbf{z}_k)$, draw predicted particles:
 $\tilde{\mathbf{x}}_k^{(i)} = \begin{cases} q_k(\cdot|\mathbf{x}_{k-1}^{(i)}, \mathbf{z}_k), & i = 1, \dots, L_{k-1}; \\ p_k(\cdot|\mathbf{z}_k), & i = L_{k-1} + 1, \dots, L_{k-1} + J_k. \end{cases}$
 and calculate the associated weights as:

$$\tilde{w}_{k|k-1}^{(i)} = \begin{cases} \frac{\tilde{\phi}_{k|k-1}(\tilde{\mathbf{x}}_k^{(i)}, \mathbf{x}_{k-1}^{(i)})}{q_k(\tilde{\mathbf{x}}_k^{(i)}|\mathbf{z}_k)} \omega_{k-1}^{(i)}, & i = 1, \dots, L_{k-1}, \\ \frac{1}{J_k} \frac{\gamma_k(\tilde{\mathbf{x}}_k^{(i)})}{p_k(\tilde{\mathbf{x}}_k^{(i)}|\mathbf{z}_k)}, & i = L_{k-1} + 1, \dots, L_{k-1} + J_k, \end{cases}$$

where

$$\tilde{\phi}_{k|k-1}(\tilde{\mathbf{x}}_k^{(i)}, \mathbf{x}_{k-1}^{(i)}) = \beta_{k|k-1}(\tilde{\mathbf{x}}_k^{(i)}|\mathbf{x}_{k-1}^{(i)}) + p_{S,k}(\mathbf{x}_{k-1}^{(i)}) f_{k|k-1}(\tilde{\mathbf{x}}_k^{(i)}|\mathbf{x}_{k-1}^{(i)}).$$

◇ Update each of the weights

$$\tilde{\omega}_k^{(i)} = \left[1 - p_{D,k}(\tilde{\mathbf{x}}_k^{(i)}) + \sum_{\mathbf{z} \in \mathbf{z}_k} \frac{\psi_{k,z}(\tilde{\mathbf{x}}_k^{(i)})}{\kappa_k(\mathbf{z}_k) + \mathcal{C}_k(\mathbf{z}_k)} \right] \tilde{w}_{k|k-1}^{(i)},$$

$$\text{where } \psi_{k,z}(\tilde{\mathbf{x}}_k^{(i)}) = p_{D,k}(\tilde{\mathbf{x}}_k^{(i)}) \eta_k(\mathbf{z}_k|\tilde{\mathbf{x}}_k^{(i)}),$$

$$\mathcal{C}_k(\mathbf{z}_k) = \sum_{j=1}^{L_{k-1}+J_k} \psi_{k,z}(\tilde{\mathbf{x}}_k^{(j)}) \tilde{w}_{k|k-1}^{(j)}.$$

◇ Calculate the total mass $\tilde{n}_{x,k} = \sum_{j=1}^{L_{k-1}+J_k} \tilde{\omega}_k^{(j)}$,

$$\text{resample } \left\{ \frac{\tilde{\omega}_k^{(i)}}{\tilde{n}_{x,k}}, \tilde{\mathbf{x}}_k^{(i)} \right\}_{i=1}^{L_{k-1}+J_k} \text{ to get } \left\{ \frac{\omega_k^{(i)}}{\tilde{n}_{x,k}}, \mathbf{x}_k^{(i)} \right\}_{i=1}^{L_k},$$

$$\text{rescale the weights by } \tilde{n}_{x,k} \text{ to get } \left\{ \omega_k^{(i)}, \mathbf{x}_k^{(i)} \right\}_{i=1}^{L_k}.$$

we can estimate the states of targets by investigating the maxima of PHD.

C. Particle PHD Filtering Algorithm

The basic idea of the Particle PHD filter is the propagation of a particle approximation to the posterior intensity function through the PHD recursion specified by (18), (19). The pseudo-code of our proposed Particle PHD filtering algorithm is described in Table I. For simplicity, we assume that the intensity of the spontaneous birth RFS Γ_k can be modeled as a Gaussian mixture of the form:

$$\gamma_k(\mathbf{x}_k) = \sum_{i=1}^{n_{\gamma,k}} p_{\gamma,k}^{(i)} N(\mathbf{x}_k; \mathbf{m}_{\gamma,k}^{(i)}, \mathbf{P}_{\gamma,k}^{(i)}) \quad (20)$$

where $n_{\gamma,k}$, $p_{\gamma,k}^{(i)}$, $\mathbf{m}_{\gamma,k}^{(i)}$, $\mathbf{P}_{\gamma,k}^{(i)}$, $i = 1, \dots, n_{\gamma,k}$, are given model parameters that determine the shape of the intensity and $N(\cdot; \cdot, \cdot)$ denotes Gaussian distribution.

D. Distributed Probability Hypothesis Density Filter

Each active sensor node maintains an identical copy of the PHD filter. Initially, they achieve this by initializing all the filters using the same random seed. To encode the multi-target states measurements at time step k , the samples obtained at time $(k - k_1)$, where k_1 denotes the length of the time interval, are propagated using multi-target states dynamic model. Assuming that $(k - k_1)$ is the last time step when the local multi-target states measurements are transmitted over the MWSN, each ac-

TABLE II
DPHD FILTERING ALGORITHM

1. Initialization

1). Initialize the Particle PHD filter at the i th active mobile sensor node, where $i = 1, 2, \dots, N_s$, using the same random seed to generate the identical particle distribution.

2). Generate the set of particles $\{\mathbf{x}_0^{(n)}\}_{n=0}^{L_0}$ for each active sensor node.

2. At time step $k \geq 1$

1). Apply the Particle PHD filtering algorithm in the local multi-target states estimation by using the local multi-target states measurement achieved by each active sensor node.

2). For the length of the vector $k_1 = 1, \dots, k$,

For the sensor node $i = 1, 2, \dots, N_s$,

i. Calculate the conditional probability $p(\mathbf{z}_k|\mathbf{b}_j, \mathbf{z}_{1:k-1}^{(n_p)})$ for the particle n_p in the measurement space using the predicted measurement and derive the Probability Mass Function (PMF) for the bins,

ii. Identify the regions where our companders need to be placed and the number of companders needed.

iii. Use one compander for each tracked target and limit the width of the companding region to $3\sigma_p^{(l)}$, where $\sigma_p^{(l)}$ denotes the standard deviation of the l th cluster.

iv. Place the compander on the mean of the l th cluster $\mu_p^{(l)}$.

v. Employ the linear quantizer for the other regions.

vi. Calculate the conditional PMF $p(\mathbf{z}_k|\mathbf{b}_j, \mathbf{z}_{1:k-1}^{(l)})$ in the transformed measurement space.

vii. Use the bin probabilities to form the Huffman tree

$H_f^{(k-1)}$ and encode the quantized measurements.

3). Remove the measurements from the queue, if the number of bits in each encoded measurement exceeds a threshold α_{th} .

4). Send the encoded measurements $\tilde{\mathbf{z}}'_k = [\tilde{\mathbf{z}}_{k-k_1}, \dots, \tilde{\mathbf{z}}_k]^T$ to all the other active mobile sensor nodes.

5). Create the Huffman tree \mathcal{T}_k to reconstruct the quantized multi-target states measurements $\tilde{\mathbf{z}}'_k$.

6). Apply the Particle PHD filter to the global multi-target state estimation by using the set $\tilde{\mathbf{z}}'_k$ of measurements.

tive sensor node constructs a histogram of the expected local multi-target states measurements, quantizes the values of the measurements, and encodes them using the Huffman encoding algorithm. The active sensor nodes then transmit the encoded multi-target states measurements to all the other active sensor nodes, which decode the data to obtain the quantized multi-target states measurements, and apply the PHD filter to get the multi-target states estimation. The pseudo-code of our proposed Distributed Probability Hypothesis Density (DPHD) filtering algorithm is provided in Table II.

1) *Proposed Quantization Scheme*: To decrease the communication overhead in the MMTT problem, we employ a nonuniform quantization scheme on the local multi-target state measurements. In our proposed quantization scheme, the construction of PMF begins by propagating the densities of the particles from time step $(k - 1)$ to k , taking the predicted-measurement error covariance matrix into account. We divide the range of the expected measurements into multiple intervals, called bins, depending on the required accuracy level, and intergrade the contribution of each propagated particle distribution over the bins to form the PMF. Letting the PMF for the appearance of the i th predicted particle $p(\mathbf{z}_k^{(i)})$ in the measurement space as follows:

$$p(\mathbf{z}_k^{(i)}) = N(\mathbf{z}_k^{(i)}; h_k(\mathbf{x}_{k|k-1}^{(i)}), \Lambda_{k|k-1}) \quad (21)$$

where $\Lambda_{k|k-1}$ denotes the predicted-measurement error covariance matrix. We define the conditional PMF for the predicted measurement $\tilde{\mathbf{z}}_k^{(i)}$ given the bin vector \mathbf{b}_j as

$$p\left(\tilde{\mathbf{z}}_k^{(i)}|\mathbf{b}_j, \mathbf{z}_{1:k-1}^{(i)}\right) \triangleq \sum_{i=1}^{L_{k-1}} \int_{\mathbf{a}_i^{(i)}}^{\mathbf{a}_{i+1}^{(i)}} p\left(\mathbf{z}_k^{(i)}\right) d\zeta \quad (22)$$

where $\mathbf{a}_i^{(i)}$ and $\mathbf{a}_{i+1}^{(i)}$ are the quantizer decision boundaries of the bin vector \mathbf{b}_j . To ensure that the target-generated measurements have smaller quantization error vector than the other measurements, we derive a nonuniform quantizer based on the PMF of the predicted multi-target states measurement, which uses the Gaussian compander given by

$$\Upsilon\left(\mathbf{z}_k^{(i)}\right) = \text{erf}\left(\frac{\mathbf{z}_k^{(i)} - \mu_p^{(l)}}{\sigma_p^{(l)}\sqrt{6}}\right) \quad (23)$$

where $\mu_p^{(l)}$ denotes the mean value of the l th cluster, $\sigma_p^{(l)}$ represents the standard deviation of the l th cluster, and $\text{erf}(x) \triangleq (2/\sqrt{\pi}) \int_0^x e^{-t^2} dt$ is the Gaussian error function.

2) *The Proposed Encoding And Decoding Scheme:* After transforming the original PMF for the appearances of the predicted particles to the companded measurement space, we create the global Huffman dictionary to encode the companded local multi-target states measurements by implementing the particle PHD filtering algorithm at each active sensor node. At each time step, we update the current particles using the quantized measurements while taking into account the additional quantization error, which has a uniform distribution with the standard deviation σ_g^2 , where σ_g^2 is determined by

$$\sigma_g^2 = \sigma_w^2 + \frac{\delta_b^2}{12} \quad (24)$$

where σ_w denotes the standard deviation of the measurement noise and δ_b^2 is the bin size.

In our proposed measurement encoding scheme, we also apply the local Huffman dictionary to reduce the number of false alarms which consume many communication resources. since the local particle PHD filters have the most updated information including the new births of the tracked targets, the target-generated measurements are most likely to have fewer number of bits than the false alarms when encoded with the local Huffman dictionary. Thus, we set an appropriate pre-defined threshold α_b for the number of bits to efficiently remove the false alarms from the set of multi-target states measurements. Then, we encode the remaining measurements using the global Huffman dictionary. To indicate whether the local multi-target states estimations will be transmitted over the MWSN, we define an indicator function $U_1^{(k)}(i)$ as follows:

$$U_1^{(k)}(i) \triangleq \begin{cases} 1, & \text{if } \mathcal{H}_{k-1}\left(\mathbf{z}_k^{(i)}\right) \leq \alpha_b; \\ 0, & \text{otherwise.} \end{cases} \quad (25)$$

In (25), $\mathcal{H}_{k-1}(\cdot)$ is a function that generates the global Huffman codes for the local multi-target states measurements.

E. Posterior Cramer-Rao Lower Bound for the Quantized Measurements

To evaluate our proposed DPHD filtering algorithm in the MMTT problem, we derive the Posterior Cramer-Rao Lower Bound (PCRLB) for the multi-target states estimation obtained through the quantized measurements.

1) *Posterior Cramer-Rao Lower Bound (PCRLB):* The estimation error covariance matrix $\Lambda_{k|k}$ for the unbiased estimator has a lower bound, called PCRLB, which is given by

$$\Lambda_{k|k} = \mathbb{E}\left[(\mathbf{x}_k - \tilde{\mathbf{x}}_{k|k})(\mathbf{x}_k - \tilde{\mathbf{x}}_{k|k})^T\right] \geq \mathcal{J}_k^{-1} \quad (26)$$

where $\mathbb{E}[\cdot]$ denotes a function of taking expectation and \mathcal{J}_k is the Fisher information matrix [15]. The matrix \mathcal{J}_{k+1} can be computed by the Riccai-like recursion as follows:

$$\mathcal{J}_{k+1} = \mathcal{W}_k^{(2,2)} - \mathcal{W}_k^{(2,1)}\left(\mathcal{J}_k + \mathcal{W}_k^{(1,1)}\right)^{-1}\mathcal{W}_k^{(1,2)} \quad (27)$$

where

$$\begin{cases} \mathcal{W}_k^{(1,1)} = \mathbb{E}\left[-\frac{\partial^2}{\partial \mathbf{x}_k^2} \log p(\mathbf{x}_{k+1}|\mathbf{x}_k)\right], \\ \mathcal{W}_k^{(1,2)} = \mathbb{E}\left[-\frac{\partial^2}{\partial \mathbf{x}_k \partial \mathbf{x}_{k+1}} \log p(\mathbf{x}_{k+1}|\mathbf{x}_k)\right], \\ \mathcal{W}_k^{(2,1)} = \mathbb{E}\left[-\frac{\partial^2}{\partial \mathbf{x}_{k+1} \partial \mathbf{x}_k} \log p(\mathbf{x}_{k+1}|\mathbf{x}_k)\right], \\ \mathcal{W}_k^{(2,2)} = \mathbb{E}\left[-\frac{\partial^2}{\partial \mathbf{x}_{k+1}^2} \log p(\mathbf{x}_{k+1}|\mathbf{x}_k)\right] \\ + \mathbb{E}\left[-\frac{\partial^2}{\partial \mathbf{x}_{k+1}^2} \log p(\tilde{\mathbf{z}}_k|\mathbf{x}_{k+1})\right]. \end{cases} \quad (28)$$

2) *PCRLB for the Quantized Measurements:* The quantized multi-target-state measurements $\tilde{\mathbf{z}}_k^{(j)}(i)$ defined in (22) satisfies $\mathbf{a}_i^{(j)} \preceq \tilde{\mathbf{z}}_k^{(j)}(i) \prec \mathbf{a}_{i+1}^{(j)}$, using (25), where $\mathbf{A} \prec \mathbf{B}$ means that the matrix \mathbf{A} is elementwise less than the matrix \mathbf{B} and $\mathbf{A} \preceq \mathbf{B}$ means that \mathbf{A} is elementwise not bigger than \mathbf{B} . Then, using (22) we derive the conditional PMF of the quantized measurements $p(\tilde{\mathbf{z}}_k^{(j)}(i)|\mathbf{x}_k)$ as follows:

$$\begin{aligned} p\left(\tilde{\mathbf{z}}_k^{(j)}(i)|\mathbf{x}_k\right) &= U_1^{(k)}(i) \Pr\left\{\mathbf{a}_i^{(j)} \preceq \tilde{\mathbf{z}}_k^{(j)}(i) \prec \mathbf{a}_{i+1}^{(j)}|\mathbf{x}_k\right\} \\ &= U_1^{(k)}(i) \Pr\left\{\mathbf{a}_i^{(j)} \preceq h_k\left(\mathbf{x}_k, \mathbf{s}_k^{(j)}\right) \right. \\ &\quad \left. + \mathbf{v}_k \prec \mathbf{a}_{i+1}^{(j)}|\mathbf{x}_k\right\} \end{aligned} \quad (29)$$

where $\mathbf{s}_k^{(j)}$ is the j th sensor's state and \mathbf{v}_k denotes the local multi-target states measurement noise at the time step k .

Assuming that \mathbf{v}_k follows the Gaussian distribution given by $\mathbf{v}_k \sim N(\cdot; 0, \sigma_w^2)$, we rewrite (30) as follows:

$$\begin{aligned} p\left(\tilde{\mathbf{z}}_k^{(j)}(i)|\mathbf{x}_k\right) &= U_1^{(k)}(i) \Pr\left\{\mathbf{a}_i^{(j)} - h_k\left(\mathbf{x}_k, \mathbf{s}_k^{(j)}\right) \preceq \right. \\ &\quad \left. \prec \mathbf{a}_{i+1}^{(j)} - h_k\left(\mathbf{x}_k, \mathbf{s}_k^{(j)}\right)|\mathbf{x}_k\right\} \end{aligned} \quad (31)$$

$$\begin{aligned} &= U_1^{(k)}(i) \int_{\mathbf{a}_i^{(j)} - h_k\left(\mathbf{x}_k, \mathbf{s}_k^{(j)}\right)}^{\mathbf{a}_{i+1}^{(j)} - h_k\left(\mathbf{x}_k, \mathbf{s}_k^{(j)}\right)} \frac{1}{\sigma_w \sqrt{2\pi}} \\ &\quad \times \exp\left(-\frac{\zeta^2}{2\sigma_w^2}\right) d\zeta \end{aligned} \quad (32)$$

$$= U_1^{(k)}(i) g_1^{(i,j)}(\mathbf{x}_k) \quad (33)$$

where

$$g_1^{(i,j)}(\mathbf{x}_k) = \Phi \left(\frac{\mathbf{a}_{l+1}^{(j)} - h_k(\mathbf{x}_k, \mathbf{s}_k^{(j)})}{\sigma_g} \right) - \Phi \left(\frac{\mathbf{a}_l^{(j)} - h_k(\mathbf{x}_k, \mathbf{s}_k^{(j)})}{\sigma_g} \right) \quad (34)$$

where $\Phi(x) \triangleq (1/\sqrt{2\pi}) \int_{-\infty}^x e^{-u^2/2} du$.

Letting $\mathcal{J}_k^{(j)}(\tilde{\mathbf{z}}_k)$ and $\tilde{\mathcal{J}}_k^{(j)}(\tilde{\mathbf{z}}_k)$ be the Fisher information matrix for the local multi-target states measurement with and without uncertainty, respectively, we have the following result:

$$\mathcal{J}_k^{(j)}(\tilde{\mathbf{z}}_k) = \tilde{\varrho}_k \tilde{\mathcal{J}}_k^{(j)}(\tilde{\mathbf{z}}_k) \quad (35)$$

where $\tilde{\varrho}_k$ is a specified system parameter, which typically depends on the probability, denoted by $p_{D,k}$, of detection, the clutter intensity λ , the standard deviation of the quantized measurement error σ_g , and the volume of the observation region V_k .

By using (33) and (34), we obtain the value of $\tilde{\mathcal{J}}_k^{(j)}(\tilde{\mathbf{z}}_k)$ as follows:

$$\tilde{\mathcal{J}}_k^{(j)}(\tilde{\mathbf{z}}_k) = \mathbb{E} \left[-\frac{\partial^2}{\partial(\mathbf{x}_{k+1})^2} \log p(\tilde{\mathbf{z}}_k^{(j)}(i) | \mathbf{x}_{k+1}) \right] \quad (36)$$

$$= \mathbb{E} \left[-\frac{\partial^2}{\partial(\mathbf{x}_{k+1})^2} \log \left\{ U_1^{(k)}(i) f_k^{(i,j)}(\mathbf{x}_k) \right\} \right] \quad (37)$$

$$= -\mathbb{E} \left[U_1^{(k)}(i) \mathcal{D}_k^{(i,j)}(\mathbf{x}_k) \right] \quad (38)$$

where

$$\mathcal{D}_k^{(i,j)}(\mathbf{x}_k) = \begin{bmatrix} \frac{\partial^2 \log g_1^{(i,j)}(\mathbf{x}_k)}{\partial(\mathbf{x}_k^{(1)})^2} & \cdots & \frac{\partial^2 \log g_1^{(i,j)}(\mathbf{x}_k)}{\partial \mathbf{x}_k^{(1)} \partial \mathbf{x}_k^{(n_x,k)}} \\ \vdots & \ddots & \vdots \\ \frac{\partial^2 \log g_1^{(i,j)}(\mathbf{x}_k)}{\partial \mathbf{x}_k^{(n_x,k)} \partial \mathbf{x}_k^{(1)}} & \cdots & \frac{\partial^2 \log g_1^{(i,j)}(\mathbf{x}_k)}{\partial(\mathbf{x}_k^{(n_x,k)})^2} \end{bmatrix}. \quad (39)$$

Using the particle PHD filtering algorithm, we can recursively derive the estimation of $\tilde{\mathcal{J}}_k^{(j)}(\tilde{\mathbf{z}}_k)$ as follows:

$$\tilde{\mathcal{J}}_k^{(j)}(\tilde{\mathbf{z}}_k) \approx -\frac{1}{T} \sum_{l=1}^T \sum_{i=1}^{\tau_k^{(j,l)}} U_1^{(k)}(i) \mathcal{D}_k^{(i,j)}(\tilde{\mathbf{x}}_k^{(l)}) \quad (40)$$

where T denotes the number of the iterations implemented in the particle PHD filtering algorithm, $\tilde{\mathbf{x}}_k^{(l)}$ is the multi-target states estimation obtained in the l th iteration. Using (35) and (40), we have the following results:

$$\begin{aligned} \mathcal{J}_k(\tilde{\mathbf{z}}_k) &= \sum_{j=1}^{N_s} \mathcal{J}_k^{(j)}(\tilde{\mathbf{z}}_k) \\ &= \tilde{\varrho}(p_{D,k}, \lambda, \sigma_g, V_k) \sum_{j=1}^{N_s} \tilde{\mathcal{J}}_k^{(j)}(\tilde{\mathbf{z}}_k) \quad (41) \\ &= -\frac{\tilde{\varrho}(p_{D,k}, \lambda, \sigma_g, V_k)}{T} \\ &\quad \times \sum_{j=1}^{N_s} \sum_{l=1}^T \sum_{i=1}^{\tau_k^{(j,l)}} U_1^{(k)}(i) \mathcal{D}_k^{(i,j)}(\tilde{\mathbf{x}}_k^{(l)}). \quad (42) \end{aligned}$$

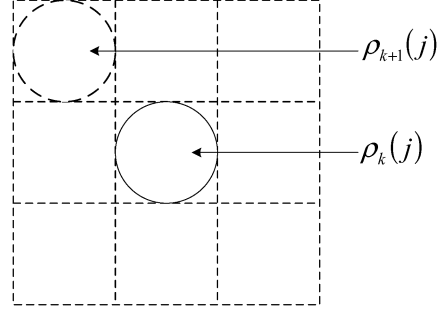


Fig. 2. Candidate locations for the j th CH at time step $(k+1)$.

IV. OPTIMAL CLUSTER HEAD (CH)-MOVEMENT CONTROL SCHEME

In our proposed mobility control system, we determine where each active CH moves based on whether the new location will increase the information gain on the multi-target states. We first predict all the possible multi-target measurements obtained from all the possible candidate locations that the CH can move to. We then treat these predicted measurements as the exact measurements, as if they were from the CHs currently located at these candidate locations. Thus, we consider the control of the CHs' movements as the problem of selecting one of the predicted measurements that are expected to obtain the maximum information gain on the multi-target states.

Considering the j th CH located at the position $\rho_k(j)$ at time step k , we assume that there are only a limited number of candidate locations that the j th CH can move to from the current position. As shown in Fig. 2, for a given grid point in the surveillance area, the set of candidate locations for the j th CH at time step $(k+1)$, $\mathcal{L}_{k+1}^{(j)}$, only includes the locations that are one step away from the current location $\rho_k(j)$, corresponding to east, north-east, north, north-west, west, south-west, south, south-east, and the current location, respectively. We use $\tilde{\mathbf{z}}_{k+1}^{(j)}(\rho_{k+1}(j))$ to denote the vector containing all the predicted multi-target states measurements made from the one-hop neighborhood of the j th CH which currently locates at $\rho_k(j)$. Letting $\mathcal{N}_k^{(j)}$ be the index-set of the one-hop neighbors of the j th CH, we simplify our problem by assuming that the j th CH uses the current multi-target states measurements from its current neighbors in $\mathcal{N}_k^{(j)}$.

A. Probabilities of Attaining the Candidate Locations

The active CH s_i selects the best candidate location $\rho_{k+1}(j) \in \mathcal{L}_{k+1}^{(j)}$ by evaluating the estimated improvement in the multi-target states estimation at time step $(k+1)$, which is calculated as follows:

$$\left\{ \begin{aligned} p(\tilde{\mathbf{x}}_{k+1} | \tilde{\mathbf{z}}_{1:k}^{(j)}) &= \int p(\tilde{\mathbf{x}}_{k+1} | \tilde{\mathbf{x}}_k) p(\tilde{\mathbf{x}}_k | \tilde{\mathbf{z}}_{1:k}^{(j)}) d\tilde{\mathbf{x}}_k, \\ p(\tilde{\mathbf{x}}_{k+1} | \tilde{\mathbf{z}}_{1:k}^{(j)}, \tilde{\mathbf{z}}_{k+1}^{(j)}(\rho_{k+1}(j))) &= \frac{p(\tilde{\mathbf{z}}_{k+1}^{(j)}(\rho_{k+1}(j)) | \tilde{\mathbf{x}}_k) p(\tilde{\mathbf{x}}_k | \tilde{\mathbf{z}}_{1:k}^{(j)})}{p(\tilde{\mathbf{z}}_{k+1}^{(j)}(\rho_{k+1}(j)) | \tilde{\mathbf{z}}_{1:k}^{(j)})}, \\ p(\tilde{\mathbf{z}}_{k+1}^{(j)}(\rho_{k+1}(j)) | \tilde{\mathbf{z}}_{1:k}^{(j)}) &= \int p(\tilde{\mathbf{z}}_{k+1}^{(j)}(\rho_{k+1}(j)) | \mathbf{x}_k) \\ &\quad \times p(\tilde{\mathbf{x}}_k | \tilde{\mathbf{z}}_{1:k}^{(j)}) d\tilde{\mathbf{x}}_{k+1} \end{aligned} \right.$$

where $\tilde{\mathbf{x}}_k$ denotes the multi-target states estimates obtained by the j th CH at the time step k , and $\tilde{\mathbf{x}}_{k+1}$ is the multi-target states estimates obtained by using the predicted measurements $\tilde{\mathbf{z}}_{k+1}^{(j)}$ at time step $(k+1)$. We define a utility function, denoted by $\varphi_l(\rho_{k+1}(j))$, as follows:

$$\varphi_l(\rho_{k+1}(j)) = \Lambda_{k+1|k+1}^{(j)}(1, 1) + \Lambda_{k+1|k+1}^{(j)}(2, 2) \quad (43)$$

where $\Lambda_{k+1|k+1}^{(j)}$ is the estimation error covariance matrix for the j th CH and $\Lambda_{k+1|k+1}^{(j)}(l, m)$ is the (l, m) -th element of the matrix $\Lambda_{k+1|k+1}^{(j)}$. Note that $\varphi_l(\rho_{k+1}(j))$ is the Mean Squared-Error (MSE) of the multi-target position estimates if choosing the candidate location $\rho_{k+1}(j)$. Then, we select the optimal candidate location by solving the following optimization problem:

$$\rho_{k+1}^*(j) = \arg \min_{\rho_{k+1}(j) \in \mathcal{L}_{k+1}^{(j)}} \{\varphi_l(\rho_{k+1}(j))\}. \quad (44)$$

Using (43), we also derive the PMF for the candidate location $\rho_{k+1}(j)$ at time step $(k+1)$ as follows:

$$p(\rho_{k+1}(j)) = \frac{\varphi_l(\rho_{k+1}(j))}{\sum_{\rho_{k+1}(j) \in \mathcal{L}_{k+1}^{(j)}} \varphi_l(\rho_{k+1}(j))}. \quad (45)$$

B. Side-Effect Impacts of CH-Movement

In our proposed CH-movement control scheme, we also consider the negative consequences due to the CHs' movements, including the additional energy consumptions, the CHs' connectivity loss, and the sensing-coverage loss. We derive the impact-weights corresponding to these negative consequences when a CH chooses to move to a candidate location.

1) *Additional Energy Consumptions:* Since the CHs spend the additional energy for the movements, it is important to ensure that the available energy is properly used to best serve the purpose of MMTT. To simplify our problem, we assume that all the active CHs move at the same constant speed. We also assume that the CH always moves along a straight line, which means that the distance that a CH moves during the interval between every two consecutive time steps is the distance between its old location and its new location. Letting $\mathcal{E}_{k+1}^{(j)}(\rho_{k+1}(j))$ be the j th CH's energy consumption on moving to the new location $\rho_{k+1}(j)$, we define $\mathcal{E}_{k+1}^{(j)}(\rho_{k+1}(j))$ as a function of the distance the j th CH moves, which is shown as follows:

$$\mathcal{E}_{k+1}^{(j)}(\rho_{k+1}(j)) = \alpha_e \|\rho_{k+1}(j) - \rho_k(j)\|_2 \quad (46)$$

where α_e is a constant, and $\|\cdot\|_2$ denotes the L_2 -norm. To characterize the side-effect of the CHs' mobility in terms of the additional energy consumption, we define the weight $w_e(\rho_{k+1}(j))$ corresponding to each candidate location $\rho_{k+1}(j)$ as follows:

$$w_e(\rho_{k+1}(j)) \triangleq \frac{\mathcal{E}_{max} - \mathcal{E}_{k+1}^{(j)}(\rho_{k+1}(j))}{\sum_{\rho_{k+1}(j) \in \mathcal{L}_{k+1}^{(j)}} (\mathcal{E}_{max} - \mathcal{E}_{k+1}^{(j)}(\rho_{k+1}(j)))} \quad (47)$$

where \mathcal{E}_{max} is a constant representing the maximum amount of energy that the CH can afford for making the one-step movement.

2) *Potential Loss of the CHs' Connections:* For the side-effect impact of the CHs' mobility, we also consider the risk that the CHs become disconnected due to their movements. To simplify our problem, we only consider the case that the CH j is disconnected with all the other CHs at the next time step $(k+1)$, which means the case that $\mathcal{N}_{k+1}^{(j)}$ is the empty set \emptyset . Letting $d_{k+1}^{(j,l)}$ denote the distance between the CHs j and l at time step $k+1$, and r_c be the communication range for the CH, we obtain the weight $w_c(\rho_{k+1}(j))$ corresponding to each candidate location $\rho_{k+1}(j)$ indicating the probability that the CH j is disconnected with all the other CHs due to moving to the new location $\rho_{k+1}(j)$ as follows:

$$\begin{aligned} w_c(\rho_{k+1}(j)) &\triangleq \sum_{\rho_{k+1}(j) \in \mathcal{L}_{k+1}^{(j)}} p(\mathcal{N}_{k+1}^{f(j)} = \emptyset | \rho_{k+1}(j)) p(\rho_{k+1}(j)) \\ &= \sum_{\rho_{k+1}(j) \in \mathcal{L}_{k+1}^{(j)}} \Pr \left\{ d_{k+1}^{(j,l)} > r_c, \forall l \in \mathcal{L}_{k+1}^{(j)} | \rho_{k+1}(j) \right\} \\ &\quad \times p(\rho_{k+1}(j)) \\ &= \sum_{\rho_{k+1}(j) \in \mathcal{L}_{k+1}^{(j)}} \left[\prod_{l \in \mathcal{N}_{k+1}^{(j)}} \Pr \left\{ d_{k+1}^{(j,l)} > r_c | \rho_{k+1}(j) \right\} \right] \\ &\quad \times p(\rho_{k+1}(j)) \\ &= \sum_{\rho_{k+1}(j) \in \mathcal{L}_{k+1}^{(j)}} \left\{ \prod_{l \in \mathcal{N}_{k+1}^{(j)}} \left[\sum_{\rho_{k+1}(l) \in \mathcal{L}_{k+1}^{(l)}} w_c^{(j,l)} \right. \right. \\ &\quad \times (\rho_{k+1}(j)) p(\rho_{k+1}(j)) \left. \left. \right] \right\} \\ &\quad \times p(\rho_{k+1}(j)) \end{aligned}$$

where $w_c^{(j,l)}(\rho_{k+1}(j))$ denotes the probability that the j th CH is disconnected at time step $(k+1)$ from its neighbor l , given that the CH j moves to the candidate location $\rho_{k+1}(j)$ and the CH l moves to the candidate location $\rho_{k+1}(l)$ at time step $(k+1)$, and

$$w_c^{(j,l)}(\rho_{k+1}(j)) = \Pr \left\{ d_{k+1}^{(j,l)} > r_c | \rho_{k+1}(l), \rho_{k+1}(j) \right\}. \quad (48)$$

To make the decision on the candidate location, the CH j is informed by the possibility of being disconnected in advance. Thus, we define $w_c^{(j,l)}(\rho_{k+1}(j, l))$ as follows:

$$w_c^{(j,l)}(\rho_{k+1}(l)) \triangleq \begin{cases} \frac{\sum_{\rho_{k+1}(l) \in \mathcal{L}_{k+1}^{(l)}} \left(\frac{1}{\alpha_c r_c - d_{k+1}^{(j,l)}} \right)}{\alpha_c r_c - d_{k+1}^{(j,l)}}, & \text{if } d_{k+1}^{(j,l)} \leq \alpha_c r_c; \\ 1, & \text{otherwise} \end{cases} \quad (49)$$

where $\alpha_c \in [0, 1]$ is a constant denoting the fraction of r_c .

3) *The Potential Loss of the Sensing Coverage:* Another potential risk arising from node movement is the potential loss of sensing coverage in certain regions of the sensing field. We represent the field of the MWSN as a 2-D grid. We denote g_t as a grid point with index t , $\mathcal{S}_k^{(t)}$ as the index-set of sensor nodes that

can detect the grid point g_t at time step k , $\tilde{e}_{k+1}^{(t,j)}(\rho_{k+1}(j))$ as the probability that the CH j covers the grid point g_t after moving to the candidate location $\rho_{k+1}(j)$ at time step $(k+1)$, $e_{k+1}^{(t)}$ as the probability that the grid node g_t is covered by at least one CH from the set $\mathcal{S}_k^{(t)}$, p_{th} as the sensing deployment control parameter representing the required sensing coverage threshold, and $\mathcal{A}(\rho_k(j))$ as the set of grid points which can be sensed by the CH j locating at the location $\rho_k(j)$.

To ensure that there is no hole in the sensing area originally covered by the sensor node j at time step k , we derive the constraint on $e_{k+1}^{(t)}$ as follows:

$$e_{k+1}^{(t)} \geq p_{th}, \quad \forall g_t \in \Delta\mathcal{A}(\rho_{k+1}(j)) \quad (50)$$

where $\Delta\mathcal{A}(\rho_{k+1}(j))$ denotes the set of grid points that will not be covered by the CH j after the CH moves to the new location $\rho_{k+1}(j)$, and

$$\Delta\mathcal{A}(\rho_{k+1}(j)) = \mathcal{A}(\rho_k(j)) \setminus \left\{ \mathcal{A}(\rho_{k+1}(j)) \cap \mathcal{A}(\rho_k(j)) \right\}. \quad (51)$$

Since calculating the expected coverage $\mathbb{E}[e_{k+1}^{(t)}]$ requires the knowledge of the set $\mathcal{S}_{k+1}^{(t)}$, which is not available to the CH j at time step k , we restrict the calculation of $\mathbb{E}[e_{k+1}^{(t)}]$ only on the CHs in the set $\mathcal{S}_k^{(t)}$, and define $\mathbb{E}[e_{k+1}^{(t)}]$ as follows:

$$\mathbb{E}[e_{k+1}^{(t)}] \triangleq 1 - \prod_{j \in \mathcal{S}_{k+1}^{(t)}} \left(1 - \sum_{\rho_{k+1}(j) \in \mathcal{L}_{k+1}^{(j)}} \tilde{e}_{k+1}^{(t,j)}(\rho_{k+1}(j)) p(\rho_{k+1}(j)) \right). \quad (52)$$

By assuming that the CHs decide their candidate location independently, we define the probability of the appearance of a hole in $\Delta\mathcal{A}(\rho_{k+1}(j))$ as $\Pr\{\exists g_t \in \Delta\mathcal{A}(\rho_{k+1}(j)) | \mathbb{E}[e_{k+1}^{(t)}] \geq p_{th}\}$. To describe the potential loss of the sensing coverage due to the CHs' mobility, we introduce the weight $w_s(\rho_{k+1}(j))$ corresponding to each candidate location at time step $(k+1)$, which represents the probability of the potential sensing-coverage loss for the CH j after moving to the new location $\rho_{k+1}(j)$. We define $w_s(\rho_{k+1}(j))$ as follows:

$$w_s(\rho_{k+1}(j)) \triangleq \frac{\sum_{g_t \in \Delta\mathcal{A}(\rho_{k+1}(j)), \mathbb{E}[\Delta e_{k+1}^{(t)}] < 0} \left| \mathbb{E}[\Delta e_{k+1}^{(t)}] \right|}{\sum_{g_t \in \Delta\mathcal{A}(\rho_{k+1}(j))} \left| \mathbb{E}[\Delta e_{k+1}^{(t)}] \right|} \times p(\rho_{k+1}(j)). \quad (53)$$

where $|\cdot|$ denotes the absolute value, and $\Delta e_{k+1}^{(t)} \triangleq e_{k+1}^{(t)} - e_k^{(t)}$.

C. CH-Movement Decision

Letting the normalized nonnegative constants C_e , C_c , and C_s , respectively, denote the costs due to the additional energy-consumption, the loss of the connectivity, and the loss of the

sensing-coverage, we define the total cost $\mathcal{C}_{k+1}^{(j)}(\rho_{k+1}(j))$ for the CH j moving to the new location $\rho_{k+1}(j)$ as follows:

$$\mathcal{C}_{k+1}^{(j)}(\rho_{k+1}(j)) \triangleq C_e w_e(\rho_{k+1}(j)) v_e + C_c w_c(\rho_{k+1}(j)) v_c + C_s w_s(\rho_{k+1}(j)) v_s \quad (54)$$

where v_e , v_c , and v_s denote the normalized weighting factors for those three side-effect impacts. By using (43) and (54), we formulate the optimization problem for our proposed CH-mobility control model as follows:

$$\begin{aligned} \min_{\rho_{k+1}(j)} \quad & \left\{ \mathcal{C}_{k+1}^{(j)}(\rho_{k+1}(j)) \right\}, \\ \text{s.t.} \quad & \rho_{k+1}(j) \in \mathcal{L}_{k+1}^{(j)}, \\ & \varphi_l(\rho_{k+1}(j)) \leq \alpha_\varphi \max_{\rho_{k+1}(j)} \{ \varphi(\rho_{k+1}(j)) \} \end{aligned} \quad (55)$$

where α_φ is the pre-defined threshold to control the size of the candidate-location set.

V. OUR CLUSTER-MEMBER ACTIVATION SCHEME

At each time step, using our proposed optimal cluster-member activation scheme, each CH activates some of the static sensor nodes locating within its communication range as its cluster members.

A. The Energy Consumption Cost Model

The communication energy consumed by the l th sensor node at the time step $(k+1)$ mainly consists of the transmitting energy $\tilde{\mathcal{E}}_{k+1,T}^{(l)}$, the receiving energy $\tilde{\mathcal{E}}_{k+1,R}^{(l)}$, the sensing energy $\tilde{\mathcal{E}}_{k+1,S}^{(l)}$, and the processing energy $\tilde{\mathcal{E}}_{k+1,P}^{(l)}$. Letting β_e be the number of bits required to encode the local multi-target states measurements, β_q denote the number of bits used by the Fusion Center (FC) to activate a sensor node for the measurement, and β_m represent the number of bits used by the sensor node to transmit its local measurement to the FC, we obtain the values of $\tilde{\mathcal{E}}_{k+1,T}^{(l)}$, $\tilde{\mathcal{E}}_{k+1,R}^{(l)}$, and $\tilde{\mathcal{E}}_{k+1,E}^{(l)}$, respectively, as follows:

$$\begin{cases} \tilde{\mathcal{E}}_{k+1,T}^{(l)} = \beta_m \left(\tilde{a}_{T,1} + \tilde{a}_{T,2} \left(\tilde{d}_{k+1}^{(l)} \right)^3 \right), \\ \tilde{\mathcal{E}}_{k+1,R}^{(l)} = \beta_q \tilde{a}_R, \\ \tilde{\mathcal{E}}_{k+1,S}^{(l)} = \beta_e \tilde{a}_{E,1}, \\ \tilde{\mathcal{E}}_{k+1,P}^{(l)} = (\beta_e + \beta_q) \tilde{a}_{E,2} \end{cases} \quad (56)$$

where $\tilde{d}_{k+1}^{(l)}$ denotes the distance between the l th sensor node and the FC at time step $(k+1)$, and $\tilde{a}_{T,1}$, $\tilde{a}_{T,2}$, \tilde{a}_R , $\tilde{a}_{E,1}$, $\tilde{a}_{E,2}$ are positive constant parameters, which represent the electronic energy consumed in transmitting one bit of data, the electronics energy related to the radio energy of the available sensor node, the electronics energy consumed in receiving one bit of data, the electronics energy consumed in sensing and encoding one bit of data, and the energy consumed in processing one bit of data, respectively.

Therefore, using (56), we obtain the energy cost for activating the l th available sensor node at the time step $(k+1)$ as follows:

$$\begin{aligned}\tilde{\mathcal{E}}_{k+1}^{(l)} &= \tilde{\mathcal{E}}_{k+1,T}^{(l)} + \tilde{\mathcal{E}}_{k+1,R}^{(l)} + \tilde{\mathcal{E}}_{k+1,S}^{(l)} + \tilde{\mathcal{E}}_{k+1,P}^{(l)} \\ &= \beta_m \left(\tilde{a}_{T,1} + \tilde{a}_{T,2} \left(\tilde{d}_{k+1}^{(l)} \right)^3 \right) + \beta_q \tilde{a}_R + \beta_e \tilde{a}_{E,1} \\ &\quad + (\beta_e + \beta_q) \tilde{a}_{E,2}.\end{aligned}\quad (57)$$

B. The Cluster-Member Activation Model

To reduce the total energy consumption, we only activate parts of the available sensor nodes at each time step while ensuring the final predicted multi-target states estimation error φ_g is below an acceptable pre-defined threshold α_{th} . In addition, letting $\mathbf{o}_{k+1} \triangleq [o_{k+1}^{(1)}, \dots, o_{k+1}^{(N_s)}]^T$ be the cluster-member activation vector, where $(o_{k+1}^{(l)} = 1)$ indicates the l th sensor node is activated at time step $(k+1)$, and $(o_{k+1}^{(l)} = 0)$ indicates that the l th sensor node is not activated at time step $(k+1)$, $\Lambda_{k+1|k+1}^{\mathbf{o}_{k+1}}$ be the estimation error covariance matrix at time step $(k+1)$ by using the cluster-member activation vector \mathbf{o}_{k+1} , we can derive the final predicted multi-target states estimation error φ_g as a function of \mathbf{o}_{k+1} as follows:

$$\varphi_g(\mathbf{o}_{k+1}) \triangleq \Lambda_{k+1|k+1}^{\mathbf{o}_{k+1}}(1,1) + \Lambda_{k+1|k+1}^{\mathbf{o}_{k+1}}(2,2) \quad (58)$$

where $\Lambda_{k+1|k+1}^{\mathbf{o}_{k+1}}(l,m)$ denotes the (l,m) th component of the matrix $\Lambda_{k+1|k+1}^{\mathbf{o}_{k+1}}$.

Since the estimation error covariance matrix $\Lambda_{k+1|k+1}^{\mathbf{o}_{k+1}}$ is not available to the FC at time step k , we approximate the matrix using the Fisher information matrix $\tilde{\mathcal{J}}_{k+1}^{(l)}$ and the predicted error covariance matrix $\Lambda_{k+1|k}^{\mathbf{o}_{k+1}}$ as follows:

$$\Lambda_{k+1|k+1}^{\mathbf{o}_{k+1}} \approx \left[\left(\Lambda_{k+1|k}^{\mathbf{o}_{k+1}} \right)^{-1} + \tilde{\mathcal{J}}_{k+1} \right]^{-1} \quad (59)$$

where

$$\tilde{\mathcal{J}}_{k+1} = \sum_{l=1}^{N_s} o_{k+1}^{(l)} \tilde{\mathcal{J}}_{k+1}^{(l)}. \quad (60)$$

Therefore, letting $\tilde{\mathcal{E}}_{k+1} \triangleq [\tilde{\mathcal{E}}_{k+1}^{(1)}, \tilde{\mathcal{E}}_{k+1}^{(2)}, \dots, \tilde{\mathcal{E}}_{k+1}^{(N_s)}]^T$, we formulate the cluster-member activation problem as a binary nonlinear programming problem as follows:

$$\begin{aligned}\min_{\mathbf{o}_{k+1}} & \left\{ \tilde{\mathcal{E}}_{k+1}^T \mathbf{o}_{k+1} \right\}, \\ \text{s.t.} & \mathbf{o}_{k+1} \in \{0,1\}^{N_s} \\ & \varphi_g(\mathbf{o}_{k+1}) \leq \alpha_t.\end{aligned}\quad (61)$$

$$(62)$$

C. Our Binary Mixed Integer Programming (MIP)-Based Cluster-Member Activation Scheme

Since $\varphi_g(\mathbf{o}_{k+1})$ is a convex function of $\mathbf{o}_{k+1} \triangleq [o_{k+1}^{(1)}, o_{k+1}^{(2)}, \dots, o_{k+1}^{(N_s)}]^T$ and $o_{k+1}^{(l)} \in [0,1]$ is the relaxation of $o_{k+1}^{(l)} \in \{0,1\}$, where $l = 1, 2, \dots, N_s$, we solve the binary nonlinear programming problem which is NP-hard by using the binary MIP technique. We represent the matrix $\Lambda_{k+1|k}^{\mathbf{o}_{k+1}}$, $(\Lambda_{k+1|k}^{\mathbf{o}_{k+1}})^{-1}$, and $\Lambda_{k+1|k+1}^{\mathbf{o}_{k+1}}$ in partitioning formats as follows:

$$\begin{cases} \Lambda_{k+1|k}^{\mathbf{o}_{k+1}} = \begin{bmatrix} \mathbf{A}_1 & \mathbf{A}_2 \\ \mathbf{A}_3 & \mathbf{A}_4 \end{bmatrix}, \\ \left(\Lambda_{k+1|k}^{\mathbf{o}_{k+1}} \right)^{-1} = \begin{bmatrix} \tilde{\mathbf{A}}_1 & \tilde{\mathbf{A}}_2 \\ \tilde{\mathbf{A}}_3 & \tilde{\mathbf{A}}_4 \end{bmatrix}, \\ \Lambda_{k+1|k+1}^{\mathbf{o}_{k+1}} = \begin{bmatrix} \mathbf{O}_1 & \mathbf{O}_2 \\ \mathbf{O}_3 & \mathbf{O}_4 \end{bmatrix} \end{cases}, \quad (63)$$

where \mathbf{A}_j , $\tilde{\mathbf{A}}_j$, and \mathbf{O}_j are 2×2 matrix, $\mathbf{A}_2 = \mathbf{A}_3^T$, $\tilde{\mathbf{A}}_2 = \tilde{\mathbf{A}}_3^T$, $\mathbf{O}_2 = \mathbf{O}_3^T$, and \mathbf{A}_1 , \mathbf{A}_4 , $\tilde{\mathbf{A}}_1$, $\tilde{\mathbf{A}}_4$, \mathbf{O}_1 , and \mathbf{B}_4 are all positive-definite matrices.

Since the active sensor nodes only transmit the information on the multi-target positions, the local Fisher information matrix $\tilde{\mathcal{J}}_{k+1}^{(l)}$ has the form as the following:

$$\tilde{\mathcal{J}}_{k+1}^{(l)} = \begin{bmatrix} \mathbf{B}^{(l)} & \mathbf{0} \\ \mathbf{0} & \mathbf{0} \end{bmatrix} \quad (64)$$

where $\mathbf{B}^{(l)}$ is a 2×2 symmetric matrix and $\mathbf{0}$ denotes a 2×2 zero matrix. Using (64) and (60), we represent the matrix $\tilde{\mathcal{J}}_{k+1}$ by

$$\tilde{\mathcal{J}}_{k+1} = \begin{bmatrix} \sum_{l=1}^{N_s} o_{k+1}^{(l)} \mathbf{B}^{(l)} & \mathbf{0} \\ \mathbf{0} & \mathbf{0} \end{bmatrix}. \quad (65)$$

Using (59) and (65), we have the results as follows:

$$\begin{cases} \mathbf{A}_1 = \left(\tilde{\mathbf{A}}_1 - \tilde{\mathbf{A}}_2 \tilde{\mathbf{A}}_4^{-1} \tilde{\mathbf{A}}_3 \right)^{-1}, \\ \mathbf{O}_1 = (\mathbf{K} + \mathbf{B})^{-1} \end{cases}, \quad (66)$$

where $\mathbf{K} \triangleq \mathbf{A}_1^{-1}$.

Letting $\tilde{k}_{i,j}$ and $\tilde{b}_{i,j}$ denote the (i,j) th component of the matrices \mathbf{K} and \mathbf{B} , respectively, we obtain the result of the final predicted multi-target states estimation error $\varphi_g(\mathbf{o}_{k+1})$ as follows:

$$\begin{aligned}\varphi_g(\mathbf{o}_{k+1}) &= \text{Tr}\{\mathbf{O}_1\} = \text{Tr}\{(\mathbf{K} + \mathbf{B})^{-1}\} \\ &= \frac{(\tilde{k}_{1,1} + \tilde{b}_{1,1}) + (\tilde{k}_{2,2} + \tilde{b}_{2,2})}{(\tilde{k}_{1,1} + \tilde{b}_{1,1})(\tilde{k}_{2,2} + \tilde{b}_{2,2}) - (\tilde{k}_{1,2} + \tilde{b}_{1,2})^2} \\ &= \left[\tilde{k}_{1,1} + \tilde{k}_{2,2} + \sum_{l=1}^{N_s} o_{k+1}^{(l)} \tilde{b}_{1,1}^{(l)} + \sum_{l=1}^{N_s} o_{k+1}^{(l)} \tilde{b}_{2,2}^{(l)} \right] \\ &\quad \times \left[\left(\tilde{k}_{1,1} + \sum_{l=1}^{N_s} o_{k+1}^{(l)} \tilde{b}_{1,1}^{(l)} \right) \left(\tilde{k}_{2,2} + \sum_{l=1}^{N_s} o_{k+1}^{(l)} \tilde{b}_{2,2}^{(l)} \right) \right. \\ &\quad \left. - \left(\tilde{k}_{1,2} + \sum_{l=1}^{N_s} o_{k+1}^{(l)} \tilde{b}_{1,2}^{(l)} \right)^2 \right]^{-1}\end{aligned}\quad (67)$$

where $\text{Tr}\{\cdot\}$ denotes the function calculating the matrix trace.

Let $\mathbf{b}_1 = [b_{1,1}^{(1)}, b_{1,1}^{(2)}, \dots, b_{1,1}^{(N_s)}]^T$, $\mathbf{b}_2 = [b_{1,2}^{(1)}, b_{1,2}^{(2)}, \dots, b_{1,2}^{(N_s)}]^T$, $\mathbf{b}_3 = [b_{2,2}^{(1)}, b_{2,2}^{(2)}, \dots, b_{2,2}^{(N_s)}]^T$, $\tilde{r}^{(l)} = 2\tilde{k}_{1,2}\tilde{b}_{1,2}^{(l)} - \tilde{k}_{1,1}\tilde{b}_{2,2}^{(l)} - \tilde{k}_{2,2}\tilde{b}_{1,1}^{(l)} + \tilde{b}_{1,1}^{(l)}/\alpha_t + \tilde{b}_{2,2}^{(l)}/\alpha_t$, $\zeta_t = \tilde{k}_{1,1}\tilde{k}_{2,2} - \tilde{k}_{1,2}^2 - \tilde{k}_{1,1}/\alpha_t - \tilde{k}_{2,2}/\alpha_t$, and $\tilde{\mathbf{D}}_{k+1} = \mathbf{b}_2 \mathbf{b}_2^T - \mathbf{b}_1 \mathbf{b}_3^T + \text{diag}(\tilde{r}^{(1)}, \tilde{r}^{(2)}, \dots, \tilde{r}^{(N_s)})$. Then, using (67), we represent the condition defined in (61) and (62) as follows:

$$\mathbf{o}_{k+1}^T \tilde{\mathbf{D}}_{k+1} \mathbf{o}_{k+1} \leq \zeta_t. \quad (68)$$

Furthermore, by introducing the new mixed variable $\{\tilde{o}_{k+1}^{(l)}\}_{l=1}^{N_s}$, we convert the condition defined in (68) as follows:

$$\begin{cases} \tilde{o}_{k+1}^{(l)} \in \mathbb{R}^+, \\ o_{k+1}^{(l)} \in \{0, 1\}, \\ \sum_{l=1}^{N_s} \left[\tilde{\mathbf{D}}_{k+1}^{(l,l')} o_{k+1}^{(l)} \right. \\ \quad \left. + \left(\tilde{D}_{k+1,1}^{(l)} - \tilde{D}_{k+1,2}^{(l)} \right) o_{k+1}^{(l)} - \tilde{D}_{k+1,1}^{(l)} \right] \leq \tilde{o}_{k+1}^{(l)}, \\ \sum_{l=1}^{N_s} \left(\tilde{D}_{k+1,1}^{(l)} o_{k+1}^{(l)} + \tilde{o}_{k+1}^{(l)} \right) \leq \zeta_t \end{cases}$$

where $\tilde{D}_{k+1,1}^{(l)}$ and $\tilde{D}_{k+1,2}^{(l)}$ are the sum of the negative and positive components of the l th row of the matrix $\tilde{\mathbf{D}}_{k+1}$, respectively.

D. Dynamic Value of the Predicted Tracking Error Threshold

To avoid checking whether the pre-defined threshold α_t is appropriate at each time step, we derive a function to determine the value of α_t dynamically, which is shown as follows:

$$\alpha_t = (1 - \beta_d)\alpha_{t,l} + \beta_d\alpha_{t,u} \quad (69)$$

where $0 < \beta_d < 1$ denotes a factor to control the desired accuracy of the multi-target states estimation, $\alpha_{t,l}$ is the lower bound of the α_t , which is obtained when all the sensor nodes are active at the time step $(k+1)$, and $\alpha_{t,u}$ represents the upper bound of the α_t , which is obtained when there is no new detection information provided at time step $(k+1)$. Equation (69) ensures that the value of the desired threshold α_t can be always met. Since $\alpha_{t,l}$ is realized when each element of the cluster-member activation vector $\mathbf{o}_k^{(l)}$ is 1 and $\alpha_{t,u}$ is realized when each element of the cluster-member activation vector $\mathbf{o}_k^{(l)}$ is 1, we derive the lower bound $\alpha_{t,l}$ and the upper bound $\alpha_{t,u}$, respectively, as follows:

$$\begin{cases} \alpha_{t,u} = \Lambda_{k+1|k}^{\mathbf{o}_{k+1}}(1, 1) + \Lambda_{k+1|k}^{\mathbf{o}_{k+1}}(2, 2), \\ \alpha_{t,l} = \frac{\tilde{k}_{1,1} + \tilde{b}_{1,1}^{(l)} + \tilde{k}_{2,2} + \tilde{b}_{2,2}^{(l)}}{(\tilde{k}_{1,1} + \tilde{b}_{1,1}^{(l)}) (\tilde{k}_{2,2} + \tilde{b}_{2,2}^{(l)}) - (\tilde{k}_{1,2} + \tilde{b}_{1,2}^{(l)})^2}. \end{cases} \quad (70)$$

VI. ASYMPTOTIC PERFORMANCE ANALYSIS

By assuming that there are at most M tracked targets at each time step, we model our MMTT problem as an M -ary hypotheses problem using N_s local detection results, where N_s denotes the number of available sensor nodes and $\{H_i\}_{i=0}^{M-1}$ represent the M hypotheses. We assume that each sensor node j makes a binary decision u_j when its detection result is $\mathbf{z}_k^{(j)}$ which is defined as follows:

$$u_j = \ell_k(\mathbf{z}_k^{(j)}) \quad (71)$$

where $\mathbf{u} = \{u_k^{(j)}\}_{j=1}^{N_s} \in \mathcal{U}$ and $\mathcal{U} = \{0, 1\}^{N_s}$. To characterize the local decision function ℓ_k , we let $R_i^{(j)}$ be the probability that the j th sensor node makes the local decision 1 when the hypothesis H_i is present. Thus, we express $R_i^{(j)}$ as follows:

$$R_i^{(j)} = \Pr\{u_j = 1|H_i\}. \quad (72)$$

We characterize the data fusion scheme at the Global Fusion Center (GFC) by using $\{\varepsilon_i\}_{i=0}^{M-1}$, where ε_i is the probability of the final-detection error when H_i is present and $l \neq i$. Thus, we can derive ε_i as follows:

$$\varepsilon_i = \sum_{l=0, l \neq i} \Pr\{D_g = H_l|H_i\} \quad (73)$$

where D_g denotes the global detection decision. Using (73), we obtain the probability of the final-detection error as follows:

$$P_e = \sum_{i=0}^{M-1} p(H_i)\varepsilon_i. \quad (74)$$

To minimize the probability of the final-detection error P_e , we derive the global detection decision as follows:

$$\begin{aligned} D_g &= \arg \max_{H_i} \{p(H_i|\mathbf{u})\} = \arg \max_{H_i} \left\{ \frac{p(\mathbf{u}|H_i)p(H_i)}{p(\mathbf{u})} \right\} \\ &= \arg \max_{H_i} \{p(\mathbf{u}|H_i)p(H_i)\} \\ &= \arg \max_{H_i} \{\log(p(\mathbf{u}|H_i)) + \log(p(H_i))\} \\ &= \arg \max_{H_i} \{\mathcal{Q}_i\} \end{aligned} \quad (75)$$

where

$$\mathcal{Q}_i \triangleq \log(p(\mathbf{u}|H_i)) + \log(p(H_i)) \quad (76)$$

where by assuming that the local multi-target state detection results are conditionally independent given the present hypothesis H_i , we can obtain:

$$\begin{aligned} p(\mathbf{u}|H_j) &= \prod_{j=1}^{N_s} p(u_j|H_j) \\ &= \prod_{j=1}^{N_s} \left(R_i^{(j)} \right)^{\frac{(1+u_j)}{2}} \left(1 - R_i^{(j)} \right)^{\frac{(1-u_j)}{2}} \\ &= \prod_{j=1}^{N_s} \left[R_i^{(j)} \left(1 - R_i^{(j)} \right) \right]^{\frac{1}{2}} \left(\frac{R_i^{(j)}}{1 - R_i^{(j)}} \right)^{\frac{u_j}{2}}. \end{aligned} \quad (77)$$

Using (77), we can rewrite \mathcal{Q}_i specified by (76) as follows:

$$\begin{aligned} \mathcal{Q}_i &= \log p(H_i) + \frac{1}{2} \sum_{j=1}^{N_s} \log \left[R_i^{(j)} \left(1 - R_i^{(j)} \right) \right] \\ &\quad + \frac{1}{2} \sum_{j=1}^{N_s} u_j \log \left(\frac{R_i^{(j)}}{1 - R_i^{(j)}} \right) \\ &= \varsigma_i^{(0)} + \sum_{j=1}^{N_s} \varsigma_i^{(j)} u_j \end{aligned} \quad (78)$$

where $i = 0, 1, \dots, M-1$, $j = 1, 2, \dots, N_s$, and

$$\begin{cases} \varsigma_i^{(0)} = \log p(H_i) + \frac{1}{2} \sum_{j=1}^{N_s} \log \left[R_i^{(j)} \left(1 - R_i^{(j)} \right) \right], \\ \varsigma_i^{(j)} = \frac{1}{2} \log \frac{R_i^{(j)}}{1 - R_i^{(j)}}. \end{cases} \quad (79)$$

Plugging (75)–(78) into (73), we can derive ε_i as follows:

$$\begin{aligned}
\varepsilon_i &= \sum_{l=0, l \neq i}^{M-1} \Pr\{D_g = H_l | H_i\} \\
&= \sum_{l=0, l \neq i}^{M-1} \Pr\{\mathcal{Q}_l = \max\{\{\mathcal{Q}_j\}_{j=0}^{M-1}\} | H_i\} \\
&= \sum_{l=0, l \neq i}^{M-1} \left[\sum_{\mathbf{u} \in \mathcal{U}} p(\mathbf{u} | H_i) \Pr\{\mathcal{Q}_l = \max\{\{\mathcal{Q}_j\}_{j=0}^{M-1}\} | \mathbf{u}\} \right] \\
&= \sum_{l=0, l \neq i}^{M-1} \left\{ \sum_{\mathbf{u} \in \mathcal{U}} p(\mathbf{u} | H_i) \left[\prod_{m=0, m \neq l}^{M-1} U_2\left(\zeta_l^{(0)} - \zeta_m^{(0)}\right) \right. \right. \\
&\quad \left. \left. + \sum_{j=1}^{N_s} \left(\zeta_l^{(j)} - \zeta_m^{(j)}\right) u_j \right] \right\} \quad (80)
\end{aligned}$$

where $U_2(\cdot)$ is the indicator function which is defined as follows:

$$U_2(x) = \begin{cases} 1, & \text{if } x > 0; \\ 0, & \text{otherwise.} \end{cases} \quad (81)$$

To simplify our local multi-target states decision scheme, we assume that, given that one hypothesis H_i is present, all the available sensor nodes have the identical local decision function ℓ_k . Thus, for an arbitrary sensor node's index j , we have the following result:

$$R_i^{(j)} = R_i. \quad (82)$$

Using (82), we simplify (79) as follows:

$$\begin{cases} \zeta_i^{(0)} = \log p(H_i) + \frac{N_s}{2} \log [R_i(1-R_i)], \\ \zeta_i^{(j)} = \zeta_i = \frac{1}{2} \log \frac{R_i}{1-R_i}. \end{cases} \quad (83)$$

Therefore, we simplify ε_i given in (80) as follows:

$$\varepsilon_i = \sum_{l=0, l \neq i}^{M-1} \left\{ \sum_{j=T_l^{\min}}^{T_l^{\max}} \binom{N_s}{j} (R_i)^j (1-R_i)^{N_s-j} \right\} \quad (84)$$

where $\binom{N_s}{j}$ is the binomial coefficient, and

$$\mathcal{T}_{i,m} = \frac{\log \frac{p(H_i)}{p(H_m)} + N_s \log \frac{1-R_i}{1-R_m}}{\log \frac{R_m(1-R_i)}{R_i(1-R_m)}}. \quad (85)$$

We further define:

$$\begin{cases} T_l^{\min} = \max_{m=0, \dots, M-1} \{\lceil \mathcal{T}_{i,m} \rceil\}, \\ T_l^{\max} = \min_{m=i, \dots, M-1} \{\lfloor \mathcal{T}_{i,m} \rfloor\}. \end{cases} \quad (86)$$

Lemma 1: Assuming that all the available sensor nodes employ the identical local decision schemes, the probability of the final-detection error P_e converges to zero at least as fast as exponentially as $N_s \rightarrow \infty$.

Proof: Using (84), we obtain the detection probability $P_{d,i}$ of the hypothesis H_j as follows:

$$P_{d,i} = \sum_{j=T_l^{\min}}^{T_l^{\max}} \binom{N_s}{j} (R_i)^j (1-R_i)^{N_s-j}. \quad (87)$$

Using the DeMoivre-Laplace Theorem [18], we obtain the asymptotic value of the detection probability $P_{d,i}$ as follows:

$$\lim_{N_s \rightarrow \infty} P_{d,i} = \lim_{N_s \rightarrow \infty} \left\{ \Phi \left(\frac{T_l^{\max} - N_s R_i}{\sqrt{N_s R_i (1-R_i)}} \right) - \Phi \left(\frac{T_l^{\min} - N_s R_i}{\sqrt{N_s R_i (1-R_i)}} \right) \right\} \quad (88)$$

where $\Phi(x)$ denotes the cumulative distribution function of the Gaussian random variable x . When the number of available sensor nodes N_s is sufficiently large, using (85) and (86), we get the following results:

$$\begin{cases} T_l^{\max} = \lfloor \mathcal{T}_{i,i+1} \rfloor > \mathcal{T}_{i,i+1} - 1, \\ T_l^{\min} = \lceil \mathcal{T}_{i,i-1} \rceil < \mathcal{T}_{i,i-1} + 1. \end{cases} \quad (89)$$

Therefore, we obtain the following inequalities:

$$\begin{cases} \frac{T_l^{\max} - N_s R_i}{\sqrt{N_s R_i (1-R_i)}} > \frac{A_{i,i+1} + N_s B_{i,i+1} - 1}{\sqrt{N_s R_i (1-R_i)}}, \\ \frac{T_l^{\min} - N_s R_i}{\sqrt{N_s R_i (1-R_i)}} < \frac{A_{i,i-1} + N_s B_{i,i-1} + 1}{\sqrt{N_s R_i (1-R_i)}} \end{cases} \quad (90)$$

where

$$\begin{cases} A_{l,m} = \frac{\log \frac{p(H_l)}{p(H_m)}}{\log \frac{R_m(1-R_l)}{R_l(1-R_m)}}, \\ B_{l,m} = \frac{1}{1 + \frac{\log \frac{R_m}{R_l}}{\log \frac{1-R_l}{1-R_m}}} - R_l. \end{cases} \quad (91)$$

By assuming $R_{i+1} > R_i > R_{i-1}$, we can get the following:

$$\begin{cases} B_{i,i+1} = \left(1 + \frac{\log \frac{R_{i+1}}{R_i}}{\log \frac{1-R_i}{1-R_{i+1}}} \right)^{-1} - R_i > 0, \\ B_{i,i-1} = \left(1 + \frac{\log \frac{R_{i-1}}{R_i}}{\log \frac{1-R_i}{1-R_{i-1}}} \right)^{-1} - R_i < 0. \end{cases} \quad (92)$$

Since $A_{i,i+1}$ and $A_{i,i-1}$ are both lower-bounded, using (90)–(92), we can get the following results:

$$\begin{cases} \lim_{N_s \rightarrow \infty} \Phi \left(\frac{T_l^{\max} - N_s R_i}{\sqrt{N_s R_i (1-R_i)}} \right) = \lim_{N_s \rightarrow \infty} \frac{A_{i,i+1} + N_s B_{i,i+1} - 1}{\sqrt{N_s R_i (1-R_i)}} = 1, \\ \lim_{N_s \rightarrow \infty} \Phi \left(\frac{T_l^{\min} - N_s R_i}{\sqrt{N_s R_i (1-R_i)}} \right) = \lim_{N_s \rightarrow \infty} \frac{A_{i,i-1} + N_s B_{i,i-1} + 1}{\sqrt{N_s R_i (1-R_i)}} = 0. \end{cases} \quad (93)$$

Using (93), we obtain the asymptotic performance of the detection probability as follows:

$$\lim_{N_s \rightarrow \infty} P_{d,i} = 1. \quad (94)$$

From (88), we have the following results:

$$\begin{aligned} \lim_{N_s \rightarrow \infty} \varepsilon_i &= 1 - \lim_{N_s \rightarrow \infty} P_{d,i} \\ &= 1 - \lim_{N_s \rightarrow \infty} \left\{ \Phi \left(\frac{T_l^{\max} - N_s R_i}{\sqrt{N_s R_i (1-R_i)}} \right) \right\} \end{aligned} \quad (95)$$

$$\begin{aligned}
 & -\Phi \left(\frac{T_i^{min} - N_s R_i}{\sqrt{N_s R_i (1 - R_i)}} \right) \Bigg\} \quad (96) \\
 & \leq \lim_{N_s \rightarrow \infty} \tau_1(N_s) + \lim_{N_s \rightarrow \infty} \tau_2(N_s) \quad (97)
 \end{aligned}$$

where

$$\begin{cases} \tau_1(N_s) = 1 - \Phi \left(\frac{A_{i,i+1} + N_s B_{i,i+1} - 1}{\sqrt{N_s R_i (1 - R_i)}} \right), \\ \tau_2(N_s) = \Phi \left(\frac{A_{i,i-1} + N_s B_{i,i-1} + 1}{\sqrt{N_s R_i (1 - R_i)}} \right). \end{cases} \quad (98)$$

Since cumulative distribution function $\Phi(x)$ has the following property:

$$\Phi(x) = 1 - \Phi(-x) \quad (99)$$

we express $\tau_2(N_s)$ defined in (98) as follows:

$$\tau_2(N_s) = 1 - \Phi \left(\frac{-A_{i,i-1} - N_s B_{i,i-1} - 1}{\sqrt{N_s R_i (1 - R_i)}} \right). \quad (100)$$

When the number, denoted by N_s , of available mobile sensor nodes is large enough such that

$$N_s > \frac{A_{i,j+1} + A_{i,j-1}}{B_{i,j+1} + B_{i,j-1}} \quad (101)$$

we obtain the following results:

$$\begin{cases} \frac{A_{i,i+1} - N_s B_{i,i+1} - 1}{\sqrt{N_s}} < \frac{-A_{i,i-1} - N_s B_{i,i-1} - 1}{\sqrt{N_s}}, & \text{if } B_{i,i+1} + B_{i,i-1} < 0; \\ \frac{A_{i,i+1} - N_s B_{i,i+1} - 1}{\sqrt{N_s}} > \frac{-A_{i,i-1} - N_s B_{i,i-1} - 1}{\sqrt{N_s}}, & \text{otherwise.} \end{cases}$$

Since $1 - \Phi(x)$ monotonically decreases for $x > 0$, we obtain the followings:

$$\begin{cases} \lim_{N_s \rightarrow \infty} \varepsilon_i < 2 \lim_{N_s \rightarrow \infty} \tau_1(N_s), & \text{if } B_{i,i+1} + B_{i,i-1} < 0; \\ \lim_{N_s \rightarrow \infty} \varepsilon_i < 2 \lim_{N_s \rightarrow \infty} \tau_2(N_s), & \text{otherwise.} \end{cases} \quad (102)$$

Therefore, we obtain the upper-bounds for $\tau_1(N_s)$ and $\tau_2(N_s)$, respectively, as follows:

$$\begin{aligned}
 \tau_1(N_s) & < \frac{\sqrt{N_s R_i (1 - R_i)} \exp \left(-\frac{[(A_{i,i+1} - 1) + N_s B_{i,i+1}]^2}{2N_s R_i (1 - R_i)} \right)}{\sqrt{2\pi} [(A_{i,i+1} - 1) + N_s B_{i,i+1}]} \\
 & < \frac{\sqrt{R_i (1 - R_i)} \exp \left(-\frac{N_s B_{i,i+1}^2 + 2B_{i,i+1}(A_{i,i+1} - 1)}{2R_i (1 - R_i)} \right)}{\sqrt{\frac{2\pi}{N_s}} [(A_{i,i+1} - 1) + N_s B_{i,i+1}]}
 \end{aligned}$$

and

$$\begin{aligned}
 \tau_2(N_s) & < \frac{\sqrt{N_s R_i (1 - R_i)} \exp \left(-\frac{[(A_{i,i-1} - 1) + N_s B_{i,i-1}]^2}{2N_s R_i (1 - R_i)} \right)}{\sqrt{2\pi} [(A_{i,i-1} - 1) + N_s B_{i,i-1}]} \\
 & < \frac{\sqrt{R_i (1 - R_i)} \exp \left(-\frac{N_s B_{i,i-1}^2 + 2B_{i,i-1}(A_{i,i-1} - 1)}{2R_i (1 - R_i)} \right)}{\sqrt{\frac{2\pi}{N_s}} [(A_{i,i-1} - 1) + N_s B_{i,i-1}]}
 \end{aligned}$$

Therefore, for any tracked target's index i , we have the following results:

$$\varepsilon_i = \mathcal{O}(e^{-N_s} / \sqrt{N_s}) \quad (103)$$

$$\lim_{N_s \rightarrow \infty} \varepsilon_i = 0. \quad (104)$$

Using (74) and (104), we can obtain the asymptotic value for the probability of the final-detection error P_e as follows:

$$\lim_{N_s \rightarrow \infty} P_e = \sum_{i=0}^{M-1} \left\{ p(H_i) \lim_{N_s \rightarrow \infty} \varepsilon_i \right\} = 0. \quad (105)$$

Since for any tracked target's index i , ε_i converges to zero at least as fast as exponentially as $N_s \rightarrow \infty$, and P_e is a linear combination of $\{\varepsilon_i\}_{i=0}^{M-1}$, it also converges to zero with the rate equal to or even faster than exponential as $N_s \rightarrow \infty$. Thus, we complete the proof. \blacksquare

VII. PERFORMANCE EVALUATIONS

In the followings, we present the simulation results of our proposed adaptive control system for the MMTT problem in our two-tier hierarchical MWSN which consists of 10 static sensors per $1m^2$ surveillance region and 5 mobile sensors totally. In our MMTT problem, each target moves according to the linear Gaussian dynamics in (13), and the initial target states are set to be $\mathbf{x}_0^{(1)} = [250, 250, 0, 0]^T$ and $\mathbf{x}_0^{(2)} = [-250, -250, 0, 0]^T$. The existing targets survive with the probability equal to $p_{S,k} = 0.98$, and the new targets appear according to a Poisson point process with the intensity function $\gamma_k = 0.1N(\cdot; \mathbf{m}_{\gamma,k}^{(1)}, \mathbf{P}_{\gamma,k}) + 0.1N(\cdot; \mathbf{m}_{\gamma,k}^{(2)}, \mathbf{P}_{\gamma,k})$, where $\mathbf{m}_{\gamma,k}^{(1)} = [150, 150, 0, 0]^T$, $\mathbf{m}_{\gamma,k}^{(2)} = [-150, -150, 0, 0]^T$, and $\mathbf{P}_{\gamma,k} = \text{diag}(100, 100, 25, 25)$.

To track multiple targets in a 2-D surveillance region, the sensing measurements with 2-degree freedom is necessary and sufficient. According to the above requirement, we employ a 2-D sensing model consisting of: 1) the sensor's orientation angle and 2) signal strength during the transmission from the targets to sensors. For simplicity, we assume that all sensors are homogenous and have the same Field Of View (FOV) region, and the model for the measurement, denoted by a vector variable $\mathbf{z}_k^{(i)}$, of the i th sensor at time k is described as follows:

$$\mathbf{z}_k^{(i)} \triangleq \begin{cases} \begin{bmatrix} \arctan \frac{y_k - l_{i2}}{x_k - l_{i1}} \\ \min \left(\xi_0 + b, \frac{\xi_0}{D} + b \right) \end{bmatrix} + \varepsilon_k, & \text{if } (x_k, y_k) \in V_m \\ \mathbf{0}, & \text{otherwise} \end{cases} \quad (106)$$

where V_m denotes the sensing region of the sensor, ε_k is the measurement noise, the first component of the sensing model denotes the horizontal shifts of the tracked targets, $[x_k, y_k]^T$ denotes the location of one tracked target, $\mathbf{L}_i = [l_{i1}, l_{i2}]^T$ denotes the location of the i th sensor, D denotes the distance between the i th sensor and the tracked target, r_s denotes the sensing range of each sensor, θ_i denotes the orientation angle of the i th sensor, and ξ_0 denotes the initial value of the signal strength generated by the target. Here we assign the values of the parameters as follows: $\xi_0 = 291.34$ nJ, $b = 61.45$ nJ, the measurement

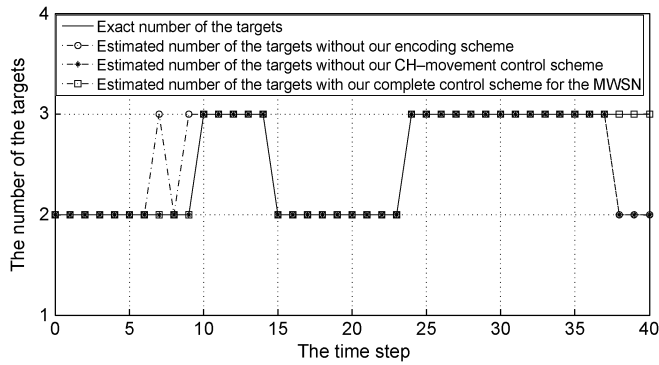


Fig. 3. Estimated number of the tracked targets versus the time steps in different cases.

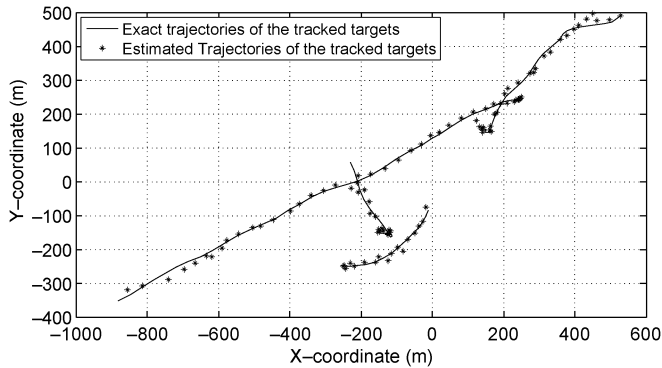


Fig. 4. The exact trajectories and the estimated trajectories of the tracked targets.

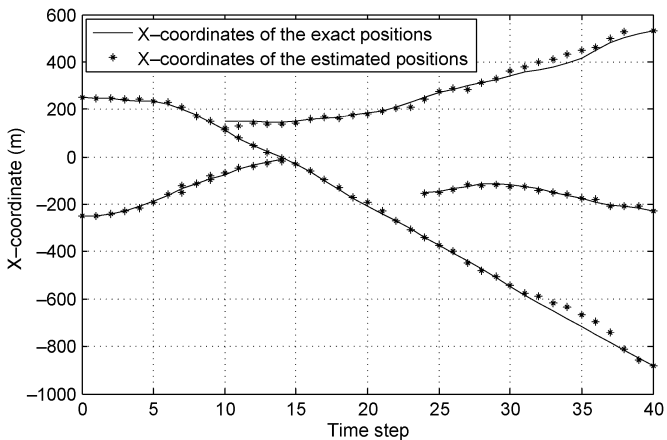


Fig. 5. The x-coordinates of the exact and the estimated positions of the tracked targets.

noise $\varepsilon_k \sim N(\cdot; \mathbf{0}, \mathbf{R}_k)$ with the mean vector $\mathbf{0}$, covariance matrix $\mathbf{R}_k = \text{diag}(\sigma_\theta^2, \sigma_s^2)$, $\sigma_\theta = 0.0001$, $\sigma_s = 2$ nJ, $r_s = 50$ m and $\Theta = \pi/4$.

In our simulations, the maximum of the detection probability $p_{D,k}$ is 0.95 and the clutter intensity $\kappa = 50/(352.79\pi)$. Fig. 3 plots the exact number of the targets in the first 40 time steps, and its estimations in the three different cases: 1) without using our encoding scheme, 2) without using our optimal CH-movement control scheme, and 3) using our complete MWSN-based control system. As shown in Fig. 3, without using our encoding scheme, the estimated number of the targets is more than the exact number at some time steps. This is caused by treating the false alarms as the measurements generated by the tracked

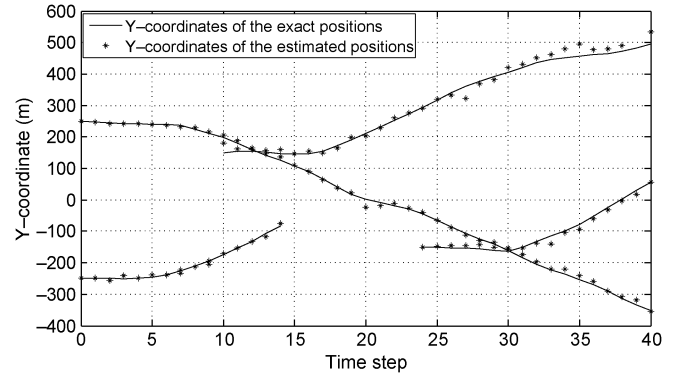


Fig. 6. The y-coordinates of the exact and the estimated positions of the tracked targets.

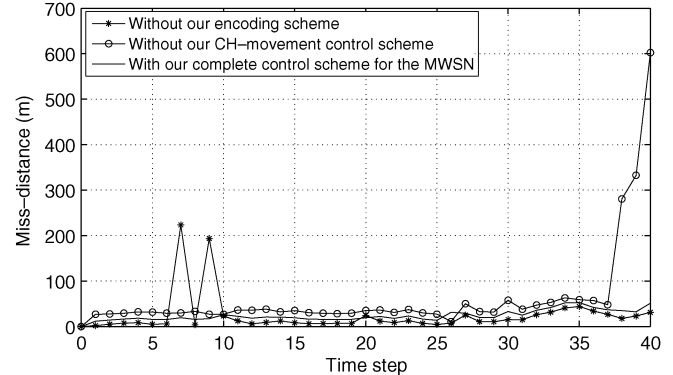


Fig. 7. Miss-distance of the multi-target states estimation versus time steps in different cases.

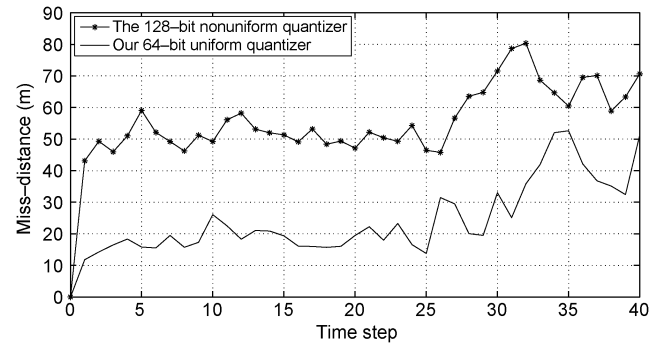


Fig. 8. Miss-distance of the multi-target states estimation versus time steps when using different types of quantizers.

targets by mistake. We can also observe that without our optimal CH-movement control scheme, our tracking scheme fails to detect some of the targets at some time steps. This happens when some of the targets travel out of the coverage of the wireless sensor network. Thus, our encoding scheme efficiently decreases the interferences of the false alarms to the final multi-target states estimations, and our proposed optimal CH-movement control system helps to ensure all the tracked targets locate within the coverage of our MWSN. Fig. 4 plots the exact and the estimated trajectories during the first 40 time steps. We observe from Fig. 4 that even when some of the targets travel across each other, our proposed tracking scheme can still distinguish and detect them with high detection accuracy. The individual x - and y -coordinates of the true tracks and the estimated positions in this case are shown in Figs. 5 and 6, respectively, which show the high multi-target estimation accuracy obtained by our

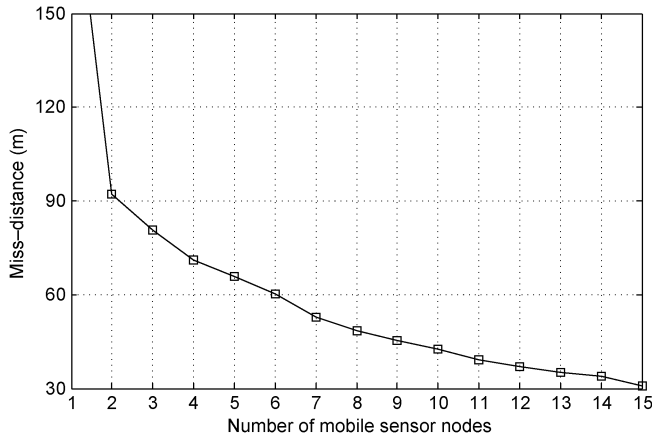


Fig. 9. Miss-distance of the multi-target states estimation versus the number of the available mobile sensor nodes.

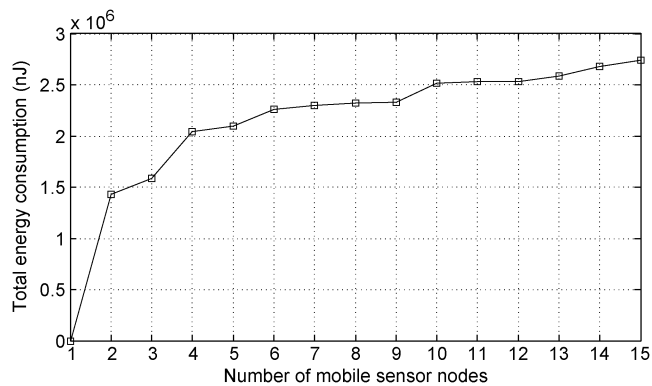


Fig. 10. Total energy consumption for the MMTT problem versus the number of the available mobile sensor nodes.

proposed control system. To evaluate the efficiency of the proposed architecture, the measurement of average performance is required. Thus, we apply the Wasserstein distance [17] as the criterion to measure the multi-target miss-distance. The Wasserstein distance between any two non-empty subsets $\hat{\mathbf{X}}$ and \mathbf{X} is defined as follows:

$$d_p(\hat{\mathbf{X}}, \mathbf{X}) = \min_{\mathbf{C}} \sqrt[p]{\sum_{i=1}^{|\hat{\mathbf{X}}|} \sum_{j=1}^{|\mathbf{X}|} C_{i,j} \|\hat{\mathbf{x}}_i - \mathbf{x}_j\|^p} \quad (107)$$

where the minimum is taken over the set of all transportation matrices \mathbf{C} (a transportation matrix is one whose entries $C_{i,j}$ satisfy $C_{i,j} \geq 0$, $\sum_{j=1}^{|\mathbf{X}|} C_{i,j} = 1/|\hat{\mathbf{X}}|$, $\sum_{i=1}^{|\hat{\mathbf{X}}|} C_{i,j} = 1/|\mathbf{X}|$). We use the Wasserstein miss-distance to validate and compare the average estimation performances of our proposed MWSN-based control scheme. Fig. 7 plots the miss-distances between the estimated multi-target states and the exact ones in the three different cases considered in Fig. 3. Fig. 7 shows that our proposed encoding scheme and the optimal CH-movement scheme efficiently get rid of the peaks of the miss-distance plots by decreasing the estimation errors in the number of the tracked targets. Fig. 8 plots the miss-distances between the estimated multi-target states and the exact ones by using our 64-bit nonuniform quantizer and the 128-bit uniform quantizer. From Fig. 8,

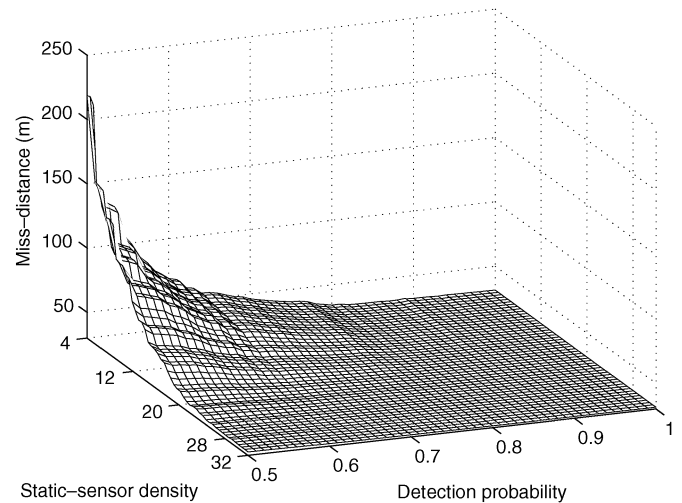


Fig. 11. Miss-distance of the multi-target states estimation versus the static-sensor density and the detection probability.

we can observe that our nonuniform quantizer outperforms the uniform one in terms of the lower number of bits and the high estimation accuracy. Figs. 9 and 10 plot the miss-distance of the measurement and the total energy consumptions versus the number of the mobile sensors acting as the CHs in our MWSN, respectively. These two figures show that as the number of the CHs increase, the miss-distance decreases exponentially while the total energy consumption increases drastically. To trade-off the high multi-target states estimation accuracy and the low energy consumption, we use 5 mobile sensors acting as the CHs in our MWSN for the MMTT problem. Fig. 11 plots the miss-distance of the multi-target states estimation versus the number of the static sensors, which act as the cluster members in our MWSN, per 1 m^2 surveillance region and the detection probabilities. As shown in Fig. 11, when the detection probability is low, we can still ensure the high multi-target state estimation accuracy by increasing the static-sensor density. In particular, for the cases with the number of static sensors larger than 20, even if the detection probability decreases to 0.5, the miss distance of our proposed scheme is still very small.

VIII. CONCLUSION

We proposed the MWSN-based control system to achieve timely and accurate mobile multi-target tracking (MMTT) with the efficient energy consumption. In particular, our proposed schemes can detect the mobile multi-targets' random appearance and disappearance in the clutter environments. We developed the optimal mutual information utility based techniques to adaptively control the locations and activations of CHs, and activations of cluster members using our Distributed Probability Hypothesis Density (DPHD) filtering algorithms. Dynamically adjusting mobile sensors' states, our schemes can efficiently improve the observabilities of the mobile targets being tracked. This is achieved by characterizing the probability-distributions distances between the multi-target states and their measurements detected/estimated/observed by sensors. We also analyzed the asymptotic performance of our proposed schemes by deriving the upper-bounds of detection-error

probabilities using DPHD algorithm. Also presented are the performance analyses, validating and evaluating our proposed adaptive control and reconfiguration schemes for MWSN in terms of multi-target states detection/estimation accuracy, energy-consumption efficiency, scalability to MWSN's size, and the robustness to the interference/noise.

REFERENCES

- [1] Y. B. Shalom and T. E. Fortmann, *Tracking and Data Association*. Boston, MA: Academic Press, 1988.
- [2] Y. B. Shalom and X. R. Li, *Multitarget-Multisensor Tracking, Principles and Techniques*. Storrs, CT: YBS Publishing, 1995.
- [3] P. Kulkarni, D. Ganesan, P. Shenoy, and Q. Lu, "SensEye: A multi-tier camera sensor network," in *Proc. Int. Conf. Multimedia*, 2005, pp. 229–238.
- [4] L. Liu, X. Zhang, and H. D. Ma, "Dynamic node collaboration for mobile target tracking in wireless camera sensor networks," in *Proc. IEEE INFOCOM 2009*, Rio De Janeiro, Brazil, Apr. 19–25, 2009, pp. 1188–1196.
- [5] R. Mahler, *Statistical Multisource-Multitarget Information Fusion*. Norwood, MA: Artech House, 2007.
- [6] R. Mahler, "Multi-target Bayes filtering via first-order multi-target moments," *IEEE Trans. Aerosp. Electron. Syst.*, vol. 39, no. 4, pp. 1152–1178, Oct. 2003.
- [7] B. Vo, S. Singh, and A. Doucet, "Sequential Monte Carlo methods for Bayesian multi-target filtering with random finite sets," *IEEE Trans. Aerosp. Electron. Syst.*, vol. 41, no. 4, pp. 1224–1245, Oct. 2005.
- [8] B. Vo and W. K. Ma, "The Gaussian mixture probability hypothesis density filter," *IEEE Trans. Signal Processing*, vol. 54, no. 11, pp. 4091–4104, Nov. 2006.
- [9] N. Whiteley, S. Singh, and S. Godsill, "Auxiliary particle implementation of the probability hypothesis density filter," in *Proc. ISPA*, 2007, pp. 1–22.
- [10] M. Vihola, "Rao-blackwellised particle filtering in random set multi-target tracking," *IEEE Trans. Aerosp. Electron. Syst.*, vol. 43, no. 2, pp. 689–705, Apr. 2007.
- [11] D. Guo and X. Wang, "Dynamic sensor collaboration via sequential Monte Carlo," *IEEE J. Selected Areas Commun.*, vol. 22, no. 6, pp. 1037–1047, Aug. 2010.
- [12] G. M. Hoffmann and C. J. Tomlin, "Mobile sensor network control using mutual information methods and particle filters," *IEEE Trans. Autom. Control*, vol. 55, no. 1, pp. 32–47, Jan. 2010.
- [13] Y. H. Hu and X. Sheng, "Dynamic sensor self-organization for distributive moving target tracking," *J. Signal Processing Syst.*, pp. 161–171, 2008.
- [14] J. Wei and X. Zhang, "Decentralized-detection based mobile multi-target tracking in wireless sensor networks," in *Proc. IEEE Int. Conf. Commun. (IEEE ICC 2010)*, Cape Town, South Africa, May 23–27, 2010, pp. 1–5.
- [15] X. Zhang and P. Willett, "Cramer-Rao bounds for discrete-time linear filtering with measurement origin uncertainties," in *Proc. Workshop Estim., Tracking Fusion*, 2001, pp. 546–560.
- [16] T. M. Cover and J. A. Thomas, *Elements of Information Theory*. New York: Wiley, 1991.
- [17] J. Hoffman and R. Mahler, "Multitarget miss distance via optimal assignment," *IEEE Trans. Syst., Man, Cybern. A*, vol. 34, no. 3, pp. 327–336, May 2004.
- [18] A. Papoulis and S. U. Pillai, *Probability, Random Variables, and Stochastic Processes*, 4th ed. Boston, MA: McGraw-Hill, 2002.



Xi Zhang (S'89–SM'98) received the B.S. and M.S. degrees from Xidian University, Xi'an, China, the M.S. degree from Lehigh University, Bethlehem, PA, all in electrical engineering and computer science, and the Ph.D. degree in electrical engineering and computer science (Electrical Engineering-Systems) from The University of Michigan, Ann Arbor.

He is currently an Associate Professor and the Founding Director of the Networking and Information Systems Laboratory, Department of Electrical and Computer Engineering, Texas A&M University,

College Station. He was an Assistant Professor and the Founding Director

of the Division of Computer Systems Engineering, Department of Electrical Engineering and Computer Science, Beijing Information Technology Engineering Institute, China, from 1984 to 1989. He was a Research Fellow with the School of Electrical Engineering, University of Technology, Sydney, Australia, and the Department of Electrical and Computer Engineering, James Cook University, Australia, under a Fellowship from the Chinese National Commission of Education. He was with the Networks and Distributed Systems Research Department, AT&T Bell Laboratories, Murray Hills, NJ, and with AT&T Laboratories Research, Florham Park, NJ. He has published more than 200 research papers in the areas of wireless networks and communications systems, mobile computing, network protocol design and modeling, statistical communications, random signal processing, information theory, and control theory and systems.

Dr. Zhang received the U.S. National Science Foundation CAREER Award in 2004 for his research in the areas of mobile wireless and multicast networking and systems. He is an IEEE Communications Society Distinguished Lecturer. He received the Best Paper Awards in the IEEE GLOBECOM 2007, IEEE GLOBECOM 2009, and IEEE WCNC 2010, respectively. He also received the TEES Select Young Faculty Award for Excellence in Research Performance from the Dwight Look College of Engineering at Texas A&M University, College Station, in 2006. He is currently serving as an Editor for the IEEE TRANSACTIONS ON COMMUNICATIONS, an Editor for the IEEE TRANSACTIONS ON WIRELESS COMMUNICATIONS, an Associate Editor for the IEEE TRANSACTIONS ON VEHICULAR TECHNOLOGY, a Guest Editor for the IEEE JOURNAL ON SELECTED AREAS IN COMMUNICATIONS for the special issue on "Broadband Wireless Communications for High Speed Vehicles," a Guest Editor for the IEEE JOURNAL ON SELECTED AREAS IN COMMUNICATIONS for the special issue on "Wireless Video Transmissions," an Associate Editor for the IEEE COMMUNICATIONS LETTERS, a Guest Editor for the IEEE COMMUNICATIONS MAGAZINE for the special issue on "Advances in Cooperative Wireless Networking," a Guest Editor for the IEEE WIRELESS COMMUNICATIONS MAGAZINE for the special issue on "Next Generation of CDMA Versus OFDMA for 4G Wireless Applications," an Editor for the *JOHN WILEY's Journal on Wireless Communications and Mobile Computing*, an Editor for the *Journal of Computer Systems, Networking, and Communications*, an Associate Editor for the *JOHN WILEY'S Journal on Security and Communications Networks*, an Area Editor for the *ELSEVIER Journal on Computer Communications*, and a Guest Editor for *JOHN WILEY'S Journal on Wireless Communications and Mobile Computing* for the special issue on "next generation wireless communications and mobile computing." He has frequently served as the Panelist on the U.S. National Science Foundation Research-Proposal Review Panels. He is serving or has served as the Technical Program Committee (TPC) Co-Chair for the IEEE INFOCOM 2013, the TPC Chair for the IEEE GLOBECOM 2011, Area TPC Chair for the IEEE INFOCOM 2012, General Co-Chair for INFOCOM 2012 - Workshop on Communications and Control for Sustainable Energy Systems: Green Networking and Smart Grids, TPC Co-Chair for IEEE ICC 2012 - Workshop on Green Communications and Networking, General Co-Chair for IEEE INFOCOM 2011 - Workshop on Green Communications and Networking, TPC Co-Chair for the IEEE ICDCS 2011 - Workshop on Data Center Performance, Panels/Demos/Posters Chairs for the ACM MobiCom 2011, TPC Vice-Chair for IEEE INFOCOM 2010, General Chair for the ACM QShine 2010, TPC Co-Chair for IEEE INFOCOM 2009 Mini-Conference, TPC Co-Chair for IEEE GLOBECOM 2008 - Wireless Communications Symposium, TPC Co-Chair for the IEEE ICC 2008 - Information and Network Security Symposium, Symposium Chair for IEEE/ACM International Cross-Layer Optimized Wireless Networks Symposium 2006, 2007, and 2008, respectively, the TPC Chair for IEEE/ACM IWCMC 2006, 2007, and 2008, respectively, the Demo/Poster Chair for IEEE INFOCOM 2008, the Student Travel Grants Co-Chair for IEEE INFOCOM 2007, the General Chair for ACM QShine 2010, the Panel Co-Chair for IEEE ICCN 2007, the Poster Chair for IEEE/ACM MSWiM 2007 and IEEE QShine 2006, Executive Committee Co-Chair for QShine, the Publicity Chair for IEEE/ACM QShine 2007 and IEEE WirelessCom 2005, and the Panelist on the Cross-Layer Optimized Wireless Networks and Multimedia Communications at IEEE ICCN 2007 and WiFi-Hotspots/WLAN and QoS Panel at IEEE QShine 2004. He has served as the TPC members for more than 100 IEEE/ACM conferences, including IEEE INFOCOM, IEEE GLOBECOM, IEEE ICC, IEEE WCNC, IEEE VTC, IEEE/ACM QShine, IEEE WoWMoM, IEEE ICCN, etc.